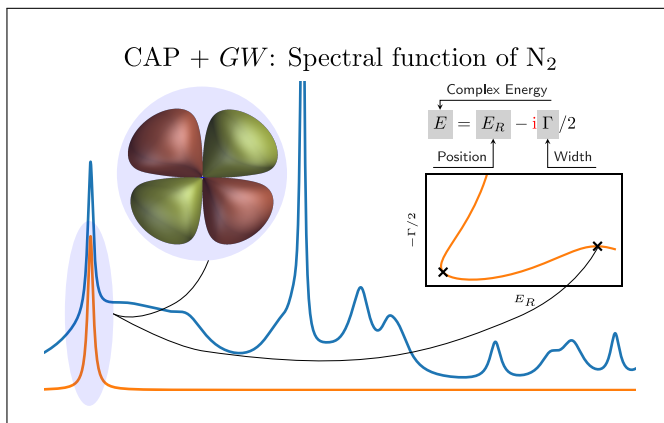


# Complex Absorbing Potential Green’s Function Methods for Resonances

Loris Burth, Fábris Kossoski, and Pierre-François Loos<sup>a)</sup>

Laboratoire de Chimie et Physique Quantiques (UMR 5626), Université de Toulouse, CNRS, Toulouse, France

The complex absorbing potential (CAP) formalism has been successfully employed in various wavefunction-based methods to study electronic resonance states. In contrast, Green’s function-based methods are widely used to compute ionization potentials and electron affinities but have seen limited application to resonances. We integrate the CAP formalism within the  $GW$  approximation, enabling the description of electronic resonances in a Green’s function framework. This approach entails a fully complex treatment of orbitals and quasiparticle energies in a non-Hermitian setting. We validate our CAP- $GW$  implementation by applying it to the prototypical shape resonances of  $N_2^-$ ,  $CO^-$ ,  $CO_2^-$ ,  $C_2H_2^-$ ,  $C_2H_4^-$ , and  $CH_2O^-$ . It offers a fast and practical route to approximate both the lifetimes and positions of resonance states, achieving an accuracy comparable to that of state-of-the-art wavefunction-based methods.



## I. INTRODUCTION

Anions can be classified as either electronically bound or unbound, based on the sign of the electron affinity (EA) of their corresponding neutral parent state.<sup>1–7</sup> Bound anions, characterized by positive EAs, can accommodate an additional electron in a square-integrable state. Two sub-classes exist. In valence-bound anions, an additional electron occupies a  $\pi^*$  or  $\sigma^*$  antibonding orbital. For example, small molecules such as  $C_2$  possess a negative lowest-unoccupied molecular orbital (LUMO) energy and can thus bind an additional electron. Valence-bound anions are even more prevalent in large  $\pi$ -conjugated systems, such as DNA, where low-energy electron attachment (0.1 eV to 0.2 eV) can weaken chemical bonds and lead to single- or double-strand breaks.<sup>8–11</sup> In dipole-bound anions (like  $NC-CH_3^-$  or  $NCH^-$ ), the extra electron resides in an extremely diffuse orbital stabilised by the long-range electric field of a permanent dipole moment (typically  $\mu \geq 2.5$  D).<sup>2,3</sup> Here, the electron remains far from the molecular core, and the binding energy is very small, often between a few meV to a few hundred meV. Such dipole-bound states are ubiquitous in water clusters, where the cumulative dipole moment is sufficient to weakly bind an electron.<sup>12</sup>

In contrast to bound anions, unbound anions possess negative EAs.<sup>7,13</sup> These anions are therefore temporary, corresponding to metastable electronic resonances, that is, discrete states embedded within the continuum that decay via electron autodetachment. Unlike bound states, which have real-valued energies, resonances are characterized by a complex (Gamow-Siegert) energy<sup>14,15</sup>

$$E = E_R - i\Gamma/2 \quad (1)$$

where  $E_R$  denotes the resonance position and  $\Gamma$  is the resonance width, which is related to the lifetime against autoionization by  $\hbar/\Gamma$ .<sup>16</sup> In the inner molecular region, these so-called Gamow-Siegert states exhibit a large amplitude similar to that of bound states. However, in the asymptotic region, their wavefunctions oscillate like those of unbound states. The complex energy leads to an exponential decay in time of the state’s amplitude, reflecting its metastable character. As a result, these states are not square-integrable, and standard Hermitian methods are inapplicable (see below).

Resonances are typically classified into two families. Shape resonances involve a one-electron process in which the excess electron is temporarily trapped in an antibonding orbital. Typical examples are the  $\Pi$ -shape resonances of  $N_2^-$  and  $CO^-$ , or electronically excited states of closed-shell anions.<sup>17–19</sup> Feshbach resonances,<sup>20–25</sup> in contrast, occur when electron attachment is accompanied by an internal electronic excitation of the molecule, resulting in

<sup>a)</sup>Electronic mail: loos@irsamc.ups-tlse.fr

a two-electron transition for detachment. A well-known example is the doubly excited  $^1\Sigma_g^+$  state of  $\text{H}_2$ .<sup>26,27</sup> This added complexity confers longer lifetimes, often extending to the microsecond range, and gives rise to much narrower spectral features. In systems such as the parabenzoquinone radical anion, both shape and Feshbach resonances manifest simultaneously.<sup>19,28–32</sup>

Temporary anions can form either through direct electron attachment to a neutral molecule or via photoexcitation of a bound anion. Their lifetimes typically span tens of femtoseconds to a few picoseconds, and they manifest spectroscopically as peaks of varying widths. These transient species play vital roles in a range of chemical and physical processes. They are implicated in DNA damage induced by ionizing radiation,<sup>8–11</sup> modulate the bioactivity of certain radiosensitizing agents,<sup>33</sup> contribute to the chemistry of the interstellar medium,<sup>34</sup> and underpin various nanofabrication technologies.<sup>35,36</sup> Beyond temporary anions, additional types of resonances include multiply charged anions, core-excited and core-ionized states, superexcited states, and Stark resonances formed when molecules are exposed to strong electric fields.<sup>37,38</sup>

Due to their dual character — exhibiting both bound and continuum-like behavior — the wavefunctions of temporary anions are not square integrable, unlike those of true bound states. This non-normalizability necessitates specialized (non-Hermitian) theoretical treatments. One of the most widely used approaches for studying shape resonances is the complex absorbing potential (CAP) method.<sup>39–47</sup> In this framework, a one-electron complex-valued potential is added to the bare Hamiltonian to effectively “absorb” the oscillatory tail of the resonance wavefunction, rendering it square integrable. This transformation allows resonances to be treated similarly to bound states, enabling the calculation of their positions and widths using adapted quantum chemistry techniques.

As with other non-Hermitian approaches, such as complex scaling<sup>48,49</sup> or the use of complex basis functions,<sup>50,51</sup> the CAP-modified Hamiltonian becomes complex-valued and non-Hermitian.<sup>37,38,52</sup> Consequently, resonances emerge directly as eigenstates of this modified Hamiltonian, each characterized by a complex energy whose imaginary part encodes the resonance width.

The CAP formalism must be coupled with a specific electronic structure method. It has been successfully combined with a broad range of wavefunction- and density-based approaches. These include selected configuration interaction (SCI),<sup>53</sup> equation-of-motion electron-attached coupled-cluster with singles and doubles (EOM-EA-CCSD),<sup>42,43,54</sup> Fock-space multireference coupled-cluster theory,<sup>55,56</sup> coupled-cluster with perturbative triples,<sup>57,58</sup> symmetry-adapted-cluster configuration interaction,<sup>59</sup> extended multiconfigurational quasidegenerate second-order perturbation theory (XMCQDPT2),<sup>30,60</sup> multireference configuration interaction (MRCI),<sup>41,61</sup> and density-functional theory (DFT).<sup>62</sup>

However, studies involving Green’s function methods in this context remain rather limited. A notable exception is

the work of Cederbaum and coworkers, who explored the combination of CAP with the second-order algebraic diagrammatic construction (ADC).<sup>63–65</sup> More recently, the third-order ADC approach was applied to paradigmatic resonances<sup>66</sup> thanks to the development of the intermediate state representation (ISR) formalism, which allows for the decoupling of the ionization potential (IP) and EA sectors via the so-called non-Dyson framework.<sup>67,68</sup>

Within the broad family of Green’s function methods,<sup>69–71</sup> the  $GW$  approximation<sup>72–74</sup> has, to the best of our knowledge, been applied to unbound anions only once.<sup>75</sup> In that study, the authors combined  $GW$  with the stabilization method by scaling the exponents of the most diffuse basis functions, then analytically continued the computed energies into the complex plane. This general framework can be applied to any electronic structure method.

This is somewhat surprising, given that  $GW$  is known to perform very well for valence<sup>76–82</sup> and core<sup>83–89</sup> IPs in molecules. In fact, the accuracy of  $GW$  is such that designing effective beyond- $GW$  schemes that outperform it at a reasonable computational cost remains a significant challenge.<sup>90–113</sup> Importantly, algorithmic improvements have been designed to lower the computational scaling of  $GW$ , which can thus be applied to very large systems.<sup>84,89,114–130</sup> However, its performance for anions, particularly unbound ones, is much less well-documented. Although some benchmark studies exist for bound anions,<sup>76–78,131–134</sup> we are not aware of any investigations addressing unbound anions using the standard non-Hermitian frameworks, such as CAP, complex scaling, or complex basis functions.

The goal of the present study is to introduce the CAP- $GW$  approach and evaluate its performance in describing shape resonances. To this end, we investigate different levels of  $GW$  self-consistency: (i) the widely used one-shot scheme, known as  $G_0W_0$ ,<sup>135–141</sup> (ii) the eigenvalue self-consistent  $GW$  (ev $GW$ ) method, in which self-consistency is enforced on the quasiparticle energies,<sup>142–146</sup> and (iii) the quasiparticle self-consistent  $GW$  (qs $GW$ ) scheme, which extends self-consistency to both the energies and orbitals.<sup>125,147–153</sup> Calculations are performed for six widely studied shape resonances in small molecules, and the resulting resonance parameters are compared against available experimental data and CAP-augmented state-of-the-art theoretical approaches, namely, CAP-SCI and CAP-EOM-EA-CCSD.

## II. THEORY

### A. Complex Absorbing Potential

When dealing with resonance states, the wave function exhibits an oscillating, non-decaying tail that prevents it from being square-integrable. To address this, a CAP is introduced into the electronic Hamiltonian. Specifically, a term  $-i\eta\hat{W}$ , with  $\eta > 0$ , is added to the original

$N$ -electron Hamiltonian  $\hat{H}$ , leading to the modified Hamiltonian

$$\hat{H}(\eta) = \hat{H} - i\eta\hat{W} \quad (2)$$

where  $\hat{W}$  is defined as a sum of one-electron contributions:

$$\hat{W} = \sum_{k=1}^N \hat{w}_k \quad (3)$$

The one-body potential  $\hat{w}_k$  can take various forms, but the most commonly employed choice is a quadratic form:

$$\hat{w}_{\alpha_k} = \begin{cases} (|\alpha_k| - \alpha_0)^2 & \text{if } |\alpha_k| > \alpha_0 \\ 0 & \text{otherwise} \end{cases} \quad (4)$$

Here,  $\hat{w}_k = \hat{w}_{x_k} + \hat{w}_{y_k} + \hat{w}_{z_k}$  sums over the Cartesian components  $\alpha_k \in \{x_k, y_k, z_k\}$  of the  $k$ th electron, and  $\alpha_0 \in \{x_0, y_0, z_0\}$  specifies the onset of the absorbing potential along each coordinate axis. The parameter  $\eta$  has dimensions of energy per length squared, ensuring that  $\eta\hat{W}$  is dimensionally consistent with the Hamiltonian. Throughout this work,  $\eta$  is given in atomic units ( $E_h a_0^{-2}$ ).

It is important to note that while  $\hat{H}$  is Hermitian, the introduction of the CAP makes  $\hat{H}(\eta)$  a complex symmetric operator, satisfying  $\hat{H}(\eta) = \hat{H}(\eta)^\top$ . As a result, the eigenvalues and eigenvectors become complex, and the left and right eigenvectors are related by simple transposition.

Due to the symmetric but non-Hermitian nature of  $\hat{H}(\eta)$ , the usual stationary principle must be adapted by replacing the standard complex inner product with the so-called *c-product*, as introduced by Moiseyev.<sup>154</sup> This leads to the following stationary expression for the complex energy:

$$E(\eta) = \langle \Psi | \hat{H}(\eta) | \Psi \rangle_c \quad (5)$$

where the trial wave function  $\Psi$  is *c-normalized* such that  $\langle \Psi | \Psi \rangle_c = 1$ , and the *c-product* is defined as

$$\langle f | g \rangle_c = \int f(\mathbf{r})g(\mathbf{r}) d\mathbf{r} \quad (6)$$

This definition ensures that the energy functional is stationary at eigenfunctions of  $\hat{H}(\eta)$ , consistent with its complex symmetric structure. In principle, with a complete basis set, the resonance energy can be obtained by taking the limit  $\eta \rightarrow 0^+$ . However, in practical calculations with finite basis sets, one must determine an optimal, small but nonzero value of  $\eta$ , denoted  $\eta_{\text{opt}}$ . This value balances two competing errors: the perturbation introduced by the CAP (which grows with  $\eta$ ) and the incompleteness error of the basis set (which diminishes with  $\eta$ ).

Riss and Meyer<sup>40</sup> proposed that  $\eta_{\text{opt}}$  can be identified by minimizing the so-called *energy velocity*:

$$\eta_{\text{opt}} = \arg \min_{\eta} \left| \eta \frac{dE(\eta)}{d\eta} \right| \quad (7)$$

Practically, this involves plotting the trajectory of  $E(\eta)$  as a function of  $\eta$  in the complex plane and locating the minimum of the energy velocity.

## B. Complex Hartree-Fock Theory

As a first step, we perform a complex restricted Hartree-Fock (cRHF) calculation incorporating the CAP to obtain a mean-field reference wave function and energy for the (closed-shell) neutral system. Therefore, we add the complex potential to the usual Fock matrix

$$\mathbf{F}(\eta) = \mathbf{F} - i\eta\mathbf{W} \quad (8)$$

where  $\mathbf{F}$  is the usual Fock matrix in the (real-valued) atomic orbital basis, which contains the one-electron core Hamiltonian, as well as the two-electron Hartree and exchange contributions. The elements of  $\mathbf{W}$  are the one-electron CAP contributions in the same basis.

Diagonalizing the  $\eta$ -dependent Fock matrix,  $\mathbf{F}(\eta)$ , yields complex molecular orbitals and energies, represented by the matrix of right eigenvectors  $\mathbf{C}(\eta)$ , which are normalized with respect to the *c-product*, such that

$$\mathbf{C}(\eta)^\top \cdot \mathbf{S} \cdot \mathbf{C}(\eta) = \mathbf{1} \quad (9)$$

Here,  $\mathbf{S}$  is the overlap of the atomic basis functions. In practice, this step is performed via a modified Cholesky decomposition.<sup>155</sup> The HF equations are iteratively solved until self-consistency is reached. To improve the convergence, we rely on Pulay's DIIS algorithm<sup>156,157</sup> adapted for complex algebra with the *c-product*. Note that we do not apply any projection to reduce the unphysical perturbation of the occupied orbitals introduced by the CAP.<sup>158</sup>

## C. Complex *GW* Approximation

As a second step, we carry out a complex-valued *GW* calculation which explicitly incorporates the CAP to access the anionic resonances starting from the neutral reference state. In this work, we present the essential equations for understanding and implementing the complex *GW* formalism, and we direct readers interested in further details to several dedicated reviews<sup>73,74,159-161</sup> and textbooks.<sup>69-71,162</sup>

Within the four-point formalism,<sup>108,163-166</sup> the instantaneous Coulomb potential is expressed as

$$v(12; 1'2') = \delta(11') \frac{\delta(t_1 - t_2)}{|\mathbf{r}_1 - \mathbf{r}_2|} \delta(22') \quad (10)$$

where  $\delta(11')$  represents the Dirac delta function. The indices, such as 1, denote shorthand notation for both time coordinates ( $t_1$ ) and the spin-space coordinates  $\mathbf{x}_1 = (\sigma_1, \mathbf{r}_1)$  for each particle.

In practical applications of the *GW* approximation, the process begins with a reference propagator  $G_0$ , typically

derived from a mean-field model. To keep things simple, we illustrate the coupled integro-differential equations for the  $GW$  formalism when  $G_0 = G_{\text{HF}}$  is used as the reference propagator. Note that, in the present context, the HF orbitals and their corresponding energies are already complex-valued (see Sec. II B).

The total self-energy can be decomposed into three components: the Hartree (H), exchange (x), and correlation (c) contributions, such that

$$\Sigma(11') = \Sigma_{\text{H}}(11') + \Sigma_{\text{x}}(11') + \Sigma_{\text{c}}(11') \quad (11)$$

The exchange-correlation part, denoted  $\Sigma_{\text{xc}} = \Sigma_{\text{x}} + \Sigma_{\text{c}}$ , is calculated as the convolution of the one-body interacting Green's function  $G$  with the dynamically screened Coulomb interaction  $W$ :

$$\Sigma_{\text{xc}}(11') = i \int d(22') G(22') W(12'; 21') \quad (12)$$

Here,  $W$  is determined via the irreducible polarizability  $\tilde{L}$  as follows:

$$\begin{aligned} W(12; 1'2') &= v(12^-; 1'2') \\ &- i \int d(343'4') W(14; 1'4') \tilde{L}(3'4'; 3^+4) v(23; 2'3') \end{aligned} \quad (13)$$

A superscript over an index, such as  $1^\pm$ , indicates an infinitesimal time shift, i.e.,  $t_{1^\pm} = t_1 \pm \tau$  ( $\tau \rightarrow 0^+$ ).

The irreducible polarizability  $\tilde{L}$  in the  $GW$  approach is approximated as the product of two Green's functions:

$$\tilde{L}(12; 1'2') = G(12') G(21') \quad (14)$$

The Green's function itself is computed via the Dyson equation:

$$G(11') = G_{\text{HF}}(11') + \int d(22') G_{\text{HF}}(12) \Sigma_{\text{c}}(22') G(2'1') \quad (15)$$

To describe quasiparticles, it is often convenient to introduce a set of spin-orbital basis functions  $\{\varphi_p\}_{1 \leq p \leq K}$  associated with energies  $\{\epsilon_p\}_{1 \leq p \leq K}$ . In the absence of a CAP, both quantities are real-valued, reflecting the Hermitian nature of the underlying operators. However, when a CAP is present, the energies and the corresponding orbitals generally become complex.

Within this spin-orbital basis, the Lehmann representation of  $G$  is given by:

$$G(\mathbf{x}_1 \mathbf{x}_{1'}; \omega) = \sum_i \frac{\varphi_i(\mathbf{x}_1) \varphi_i(\mathbf{x}_{1'})}{\omega - \epsilon_i - i\kappa} + \sum_a \frac{\varphi_a(\mathbf{x}_1) \varphi_a(\mathbf{x}_{1'})}{\omega - \epsilon_a + i\kappa} \quad (16)$$

Here, the indices  $a, b, \dots$  represent the  $V$  virtual orbitals (states above the Fermi level),  $i, j, \dots$  denote the  $O$  occupied orbitals (states below the Fermi level), and  $\nu$  labels single (de)excitation ( $ia$ ). The indices  $p, q, \dots$  are used for arbitrary orbitals, and we have  $K = O + V$ . The parameter  $\kappa > 0$  is a small positive broadening term that

ensures the correct causal structure of the Green's function. It is commonly denoted as  $\eta$  in the literature, but we use  $\kappa$  here to avoid confusion with the CAP strength parameter [see Eq. (2)].

By performing Fourier transforms and projecting onto the spin-orbital basis, we can derive the matrix elements for the correlation part of the self-energy:

$$[\Sigma_{\text{c}}(\omega)]_{pq} = \sum_{i\nu} \frac{M_{pi,\nu} M_{qi,\nu}}{\omega - \epsilon_i + \Omega_\nu - i\kappa} + \sum_{a\nu} \frac{M_{pa,\nu} M_{qa,\nu}}{\omega - \epsilon_a - \Omega_\nu + i\kappa} \quad (17)$$

The transition densities are expressed as:

$$M_{pq,\nu} = \sum_{ia} [\langle pa|qi \rangle_{\text{c}} X_{ia,\nu} + \langle pi|qa \rangle_{\text{c}} Y_{ia,\nu}] \quad (18)$$

Here, the bracket notation represents the electron repulsion integrals:

$$\langle pq|rs \rangle_{\text{c}} = \iint \frac{\varphi_p(\mathbf{x}_1) \varphi_q(\mathbf{x}_2) \varphi_r(\mathbf{x}_1) \varphi_s(\mathbf{x}_2)}{|\mathbf{r}_1 - \mathbf{r}_2|} d\mathbf{x}_1 d\mathbf{x}_2 \quad (19)$$

The excitation energies  $\Omega_\nu$ , satisfying  $\text{Re}(\Omega_\nu) > 0$ , and the corresponding amplitudes  $X_{ia,\nu}$  and  $Y_{ia,\nu}$  are obtained by solving a Casida-like random-phase approximation (RPA)<sup>167-170</sup> eigenproblem in the basis of single excitations ( $i \rightarrow a$ ) and deexcitations ( $a \rightarrow i$ ):

$$\begin{pmatrix} \mathbf{A} & \mathbf{B} \\ -\mathbf{B} & -\mathbf{A} \end{pmatrix} \cdot \begin{pmatrix} \mathbf{X} & \mathbf{Y} \\ \mathbf{Y} & \mathbf{X} \end{pmatrix} = \begin{pmatrix} \mathbf{X} & \mathbf{Y} \\ \mathbf{Y} & \mathbf{X} \end{pmatrix} \cdot \begin{pmatrix} \mathbf{\Omega} & \mathbf{0} \\ \mathbf{0} & -\mathbf{\Omega} \end{pmatrix} \quad (20)$$

Here,  $\mathbf{X}$  and  $\mathbf{Y}$  are matrices whose columns are the eigenvectors  $\mathbf{X}_\nu$  and  $\mathbf{Y}_\nu$ , respectively, and  $\mathbf{\Omega}$  is a diagonal matrix with eigenvalues  $\Omega_\nu$  on the diagonal, representing the excitation energies. The matrix elements of  $\mathbf{A}$  and  $\mathbf{B}$  are defined as

$$A_{ia,jb} = (\epsilon_a - \epsilon_i) \delta_{ij} \delta_{ab} + \langle aj|ib \rangle_{\text{c}} \quad (21a)$$

$$B_{ia,jb} = \langle ab|ij \rangle_{\text{c}} \quad (21b)$$

Unlike the usually employed complex version of Eq. (20), which involves complex conjugation of the amplitudes,<sup>171</sup> this formulation does not, owing to the use of the complex symmetric c-product in place of the standard Hermitian scalar product, such that  $\langle ij|ab \rangle_{\text{c}} = \langle ab|ij \rangle_{\text{c}}$ .

We impose the following normalization conditions on the solutions  $\mathbf{X}$  and  $\mathbf{Y}$  similar to the real case:<sup>172</sup>

$$\mathbf{X}^\top \cdot \mathbf{X} - \mathbf{Y}^\top \cdot \mathbf{Y} = \mathbf{1} \quad (22a)$$

$$\mathbf{X}^\top \cdot \mathbf{Y} - \mathbf{Y}^\top \cdot \mathbf{X} = \mathbf{0} \quad (22b)$$

#### D. Self-Consistent $GW$ Schemes

We now shift our attention to the computation of the Dyson orbitals  $\varphi_p$  and quasiparticle energies  $\epsilon_p$ . The Dyson equation (15) implies that these quantities should satisfy the following dynamical non-Hermitian equation:

$$[f + \Sigma_{\text{c}}(\omega = \epsilon_p)] \varphi_p = \epsilon_p \varphi_p \quad (23)$$

where  $f$  represents the Fock operator in the molecular orbital basis. However, the frequency dependence of the correlation self-energy  $\Sigma_c$  introduces non-linearity and complexity to this quasiparticle equation, prompting the use of various approximations.

The  $G_0W_0$  scheme, for instance, involves a single-shot iteration of Eq. (23) by considering only the diagonal elements of the self-energy.<sup>135–141</sup> In this approach, starting from one-electron HF orbitals  $\varphi_p^{\text{HF}}$  with energies  $\epsilon_p^{\text{HF}}$ , the following equation is solved:

$$\epsilon_p^{\text{HF}} + [\Sigma_c(\omega = \epsilon_p)]_{pp} = \epsilon_p \quad (24)$$

By performing a root search using the Newton-Raphson algorithm starting from the mean-field energies, we aim to locate the quasiparticle solutions, i.e., the roots of the non-linear equations that carry the largest spectral weights:

$$Z_p = \frac{1}{1 - \left. \frac{\partial \Sigma_c(\omega)}{\partial \omega} \right|_{\omega = \epsilon_p}} \quad (25)$$

In other words, the so-called satellites are discarded.

The *evGW* method takes a more iterative approach by updating, at each step, the RPA eigenvectors  $\mathbf{X}_\nu$  and  $\mathbf{Y}_\nu$  used to construct the transition densities [see Eq. (18)], the RPA neutral excitation energies  $\Omega_\nu$  and quasiparticle energies  $\epsilon_p$  involved in the expression of the RPA matrix elements [see Eqs. (21a) and (21b)] and the self-energy [see Eq. (17)]. This iterative refinement of the self-energy leads to progressively improved quasiparticle energies until convergence is achieved.<sup>142–146</sup>

In the *qsGW* approach, both orbitals and energies are updated self-consistently until convergence is reached.<sup>125,147–153</sup> This is accomplished by iteratively diagonalizing an effective Fock-like operator

$$\left( f + \tilde{\Sigma}_c \right) \varphi_p = \epsilon_p \varphi_p \quad (26)$$

where the correlation part of the self-energy is approximated by a static, Hermitian operator  $\tilde{\Sigma}_c$  with matrix elements given by

$$[\tilde{\Sigma}_c]_{pq} = \frac{[\Sigma_c(\omega = \epsilon_p)]_{pq} + [\Sigma_c(\omega = \epsilon_q)]_{qp}}{2} \quad (27)$$

A recent alternative to this approximation, based on a similarity renormalization group (SRG) approach, has been proposed.<sup>153</sup> We extended this method for complex-valued energies. The expressions for the self-energy can be found in Appendix A. The SRG regularizes the self-energy, in contrast to the approach of Eq. (27). Such regularization is crucial, as achieving convergence in a large basis set, required to treat resonances at the *qsGW* level, is generally challenging. The SRG-regularized self-energy and the form given in Eq. (27) are closely related. The former depends on a flow parameter  $s$ . In the limit  $s \rightarrow \infty$ , both yield identical diagonal components of the

self-energy, leading to very similar final results. Conversely, at  $s = 0$ , the method reduces to the mean-field approximation, recovering the corresponding orbital energies and orbitals. The same renormalization can be used for *evGW*. In the following, unless otherwise stated, we use the renormalized version of the *evGW* and *qsGW* methods to improve convergence.

As discussed in Sec. I, resonance states are characterized by complex energies with a small negative imaginary component, reflecting their finite lifetimes. To identify such a state, we first perform a calculation on the neutral molecule and then examine the quasiparticle energies  $\epsilon_p$  with real part above the Fermi level, corresponding to electron attachment processes. Among the states within a given real component energy window, the resonance is identified as the one with the smallest imaginary part, indicating the longest lifetime and the most bound-state-like character. Its position and width are given by

$$E_R = \text{Re}(\epsilon_p) \quad \Gamma = -2 \text{Im}(\epsilon_p) \quad (28)$$

in accordance with Eq. (1). These definitions apply both at the HF and the *GW* levels of theory. At the HF level, this approximation to IPs and EAs is commonly referred to as Koopmans' theorem.<sup>173</sup>

As mentioned in Sec. I, *GW* can be implemented with cubic scaling, thanks to numerous innovative algorithmic developments.<sup>84,89,114–130</sup> In particular, a cubic-scaling implementation of *qsGW* was recently reported by Förster and Visscher.<sup>125</sup> As a result, partially self-consistent *GW* schemes can now be applied to molecular systems beyond the size limit of wavefunction methods like EOM-CCSD.

## E. Spectral Function

The single-particle Green's function provides direct access to the spectral function

$$A_p(\omega) = \frac{1}{\pi} |\text{Im} G_p(\omega)| \quad (29)$$

of each quasiparticle state  $p$ , as well as to the total spectral density

$$A(\omega) = \sum_p A_p(\omega) \quad (30)$$

In  $G_0W_0$  and *evGW*, where the self-energy is  $\omega$ -dependent, the spectral function yields

$$A_p(\omega) = \frac{1}{\pi} \frac{|I(\omega)|}{R(\omega)^2 + I(\omega)^2} \quad (31)$$

with

$$R(\omega) = \text{Re} \left\{ \omega - \epsilon_p^{\text{HF}} - [\Sigma_c(\omega)]_{pp} \right\} \quad (32a)$$

$$I(\omega) = \text{Im} \left\{ \epsilon_p^{\text{HF}} + [\Sigma_c(\omega)]_{pp} - \text{sgn}[\text{Re}(\epsilon_p^{\text{HF}} - \mu)] \kappa \right\} \quad (32b)$$

For the qsGW with static self-energy, the spectral function is given by:

$$A_p(\omega) = \frac{1}{\pi} \frac{|\text{Im}\{\epsilon_p - \text{sgn}[\text{Re}(\epsilon_p - \mu)]\kappa\}|}{\text{Re}(\omega - \epsilon_p)^2 + \text{Im}\{\epsilon_p - \text{sgn}[\text{Re}(\epsilon_p - \mu)]\kappa\}^2} \quad (33)$$

In standard GW calculations, a finite broadening parameter  $\kappa$  is typically introduced to generate a non-zero width, *i.e.* finite lifetime. In our CAP-based approach, however, an imaginary part to the energies is inherently introduced, effectively regularizing the Green's function and eliminating the need for artificial broadening.

### III. COMPUTATIONAL DETAILS

The various flavours of CAP-GW developed here have been implemented in an open-source in-house program, named QUACK.<sup>174</sup> The one-electron CAP integrals have been computed with OPENCAP 1.2.7.<sup>175</sup> For the six small molecules investigated here, the CAP onsets, as well as the bond lengths and the bond angles, are given in Table I. In addition, we provide, in the [Supporting Information](#), the geometry files and basis sets. For the SRG, we systematically used  $s = 500$ , unless otherwise stated. This ensures good convergence to the result obtained without regularization.<sup>153</sup> Additionally, we employ the DIIS extrapolation using information from up to five previous iterations. The qsGW calculations are carried out with a convergence threshold of  $5 \times 10^{-4}$  a.u. on the usual commutator norm.<sup>176</sup> Under these conditions, such calculations typically converge within approximately four or five iterations. We calculate the derivatives needed to obtain the energy velocity [see Eq. (7)] by the standard second-order finite difference scheme using a step size of  $5 \times 10^{-5}$  for  $\eta$ .

The broadening parameter  $\kappa$  is set to zero in all CAP-GW calculations. Both the GW approximation and the CAP formalism are always applied to all occupied and virtual orbitals. For  $G_0W_0$  and evGW, quasiparticle energies are computed by directly solving the non-linear, frequency-dependent quasiparticle equation, without resorting to linearization. Our study is limited to closed-shell neutral reference systems, consistently employing a restricted formalism. Throughout this work, HF orbitals and energies are systematically used as the starting point, a choice justified by the relatively small size of the molecular systems considered.

For all calculations in this work, we employ the aug-cc-pVTZ+3s3p3d basis set. This corresponds to the standard aug-cc-pVTZ basis set, augmented by three additional diffuse functions of each angular momentum type (s, p, and d), centered at the geometric center of the molecule. For each angular momentum, the exponent of the first added diffuse function is chosen as half the average of the smallest exponents of the functions centered at the unique non-hydrogen atoms. The remaining two exponents for each angular momentum are generated by successively

TABLE I. Parameters employed for the CAP calculations: CAP onset ( $x_0, y_0, z_0$ ), bond lengths and angles. All lengths are in bohr and all angles in degrees. The molecular orientation with respect to the CAP can be seen in the [Supporting Information](#).

System	$(x_0, y_0, z_0)$	Bond length	Bond angle
$\text{N}_2^-$	(2.76, 2.76, 4.88)	$R_{\text{NN}} = 2.0740$	–
$\text{CO}^-$	(2.76, 2.76, 4.97)	$R_{\text{CO}} = 2.1316$	–
$\text{C}_2\text{H}_2^-$	(3.20, 3.20, 6.35)	$R_{\text{CC}} = 2.2733$ $R_{\text{CH}} = 2.0088$	$\angle_{\text{CCH}} = 180.0$
$\text{C}_2\text{H}_4^-$	(7.1, 4.65, 3.40)	$R_{\text{CC}} = 2.5303$ $R_{\text{CH}} = 2.0522$	$\angle_{\text{CCH}} = 121.2$
$\text{CH}_2\text{O}^-$	(3.85, 2.95, 6.10)	$R_{\text{CO}} = 2.2771$ $R_{\text{CH}} = 2.0995$	$\angle_{\text{HCO}} = 121.9$
$\text{CO}_2^-$	(3.33, 3.33, 9.57)	$R_{\text{CO}} = 2.1978$ $R_{\text{CH}} = 2.0995$	–

halving the previous one, forming a geometric progression. The same procedure has been used before.<sup>43,53,177</sup> Full details of the basis sets used in this study are provided in the [Supporting Information](#).

## IV. RESULTS

### A. $\text{N}_2^-$

#### 1. Context and Approach

The  $\text{N}_2^-$  temporary anion, corresponding to a  $^2\Pi_g$  configuration, is one of the most extensively studied resonances. It therefore serves as the first benchmark system for our method and is discussed in greater detail to provide the necessary context for interpreting the results of systems examined subsequently. For each system and method, we provide Dyson orbitals that confirm the electronic configuration, as well as energy-velocity plots, in the [Supporting Information](#).

We begin with a brief overview of results obtained using various related theoretical approaches. While not intended to be comprehensive, this overview serves to place our findings in the appropriate context. We then present the results obtained with the methods introduced in this work.

Starting at the lowest level of theory, we present a more qualitative discussion, as these results are inherently less accurate by design. As described in Sec. II B, we implemented a complex restricted HF method incorporating a CAP. Koopmans' theorem provides a mean-field estimate of the EA. This level of theory is highly approximate, even more so than other mean-field approaches that perform self-consistent calculations for both the neutral and anionic species. The energy difference in the latter yields the EA while accounting for state-specific orbital relaxation, commonly known as the  $\Delta\text{SCF}$  method.

$\Delta\text{SCF}$  calculations targeting the resonance require a state-specific HF formulation, which is feasible but beyond

the scope of this work. Comparing our Koopmans-level results with literature  $\Delta$ SCF data,<sup>62</sup> both methods overestimate the resonance position by roughly 1 eV, while we overestimate the width by a factor of about two. In contrast,  $\Delta$ SCF yields more reasonable widths. Nevertheless, our method successfully identifies the resonance and provides rough estimates of the position and width. Thus, it serves as a suitable mean-field starting point for subsequent  $GW$  corrections, rather than final predictive results.

At a comparable level of correlation treatment,  $GW$  methods have been combined with the stabilization technique, which estimates the position and width by analytic continuation.<sup>75</sup> In that study,  $G_0W_0$  underestimates the width obtained by EOM-CCSD with analytic continuation by more than a factor of four. In contrast, a self-consistent  $GW$  approach that includes orbital relaxation yields lifetimes of the correct order of magnitude.<sup>75</sup>

Furthermore, Green's function methods combined with CAP have been applied in previous studies using different basis sets than those employed in our work, making a direct comparison difficult. Nevertheless, these approaches have been shown to yield reasonable estimates for both the resonance position and width. For instance, reported values including basis set uncertainty are 2.58(13) eV for the position and 0.55(14) eV for the width.<sup>64</sup> Despite the methodological and basis set differences, our qsGW results for the resonance position largely fall within the reported error margins (see Table II). However, the resonance width at the second minimum (see below) deviates by 0.17 eV.

We now turn to the highest level of theory combined with a CAP: extrapolated full configuration interaction (exFCI), which treats all electronic correlations.<sup>53</sup> Due to its high computational cost, reference data are limited. For  $N_2^-$  and  $CO^-$ , however, exFCI results<sup>53</sup> are available at the optimal CAP strength  $\eta$  obtained from EOM-EA-CCSD calculations.<sup>43</sup> Comparing EOM-EA-CCSD to exFCI reveals smaller deviations than those observed between our  $GW$  results and EOM-EA-CCSD. We remark that the deviations are in the expected order of magnitude of CCSD to FCI for neutral excitations (see Table II).<sup>178</sup> Since exFCI data is available only for selected systems and lacks  $\eta$ -optimization, while EOM-EA-CCSD values exist for all systems studied in this work, we adopt CAP-EOM-EA-CCSD as our primary theoretical reference.

For  $N_2^-$ , resonance positions and widths derived by CAP-EOM-EA-CCSD have been reported at significantly different CAP strengths: One at  $\eta = 0.0015$ <sup>43</sup> and one at  $\eta = 0.007$ .<sup>179</sup> Those values correspond to two different local minima in the energy velocity. We observe a qualitatively similar behavior and trajectory using the qsGW method (see Fig. 1). Similar multiple-minimum structures also appear in other systems studied. This phenomenon appears to reflect a broader issue within the CAP framework, which, to our knowledge, remains unresolved. While solving this issue is beyond the scope of the present work, our goal is to assess the performance

of CAP- $GW$  approaches relative to higher-level theories. For  $N_2^-$ , we analyze both reported minima. For the remaining systems, multiple minima are mentioned when encountered, but we report only the results that correspond to the CAP-EOM-EA-CCSD reference.

## 2. Trajectories, Positions and Lifetimes

Within the qsGW framework, a single state can be followed continuously along the  $\eta$ -trajectory to identify both minima. In contrast, for methods based on HF orbitals, such as  $G_0W_0$  and  $evGW$ , two distinct trajectories must be tracked (see Fig. 1). These apparently describe the same resonance state, but at different values of  $\eta$ . Moreover, for these HF-based methods, no local minimum is found in the vicinity of the first reported minimum, except at the Koopmans level of theory, at  $\eta = 0.0017$ . We therefore adopt this value to estimate the resonance parameters in  $G_0W_0$  and  $evGW$ .

Also, in  $evGW$ , the  $\eta$ -trajectory was not smooth enough to reliably identify the second reported minimum of the energy velocity using finite differences. We thus performed additional calculations with  $s = 100$  to identify the optimal  $\eta$  value.

Our results are presented in Table II. We find that all discussed  $GW$  methods overestimate the resonance position compared to reference theoretical methods and experiment. While the  $G_0W_0$  and  $evGW$  methods deviate by approximately 0.5 eV from the CAP-EOM-EA-CCSD reference for the first minimum, they are only off by about 0.1 eV for the second minimum. On the other hand, these methods yield a more accurate lifetime for the first minimum than for the second. The qsGW method, by contrast, closely reproduces the reference values, with differences of about 0.1 eV for the resonance position and 0.05 eV for the width  $\Gamma$ . Compared to experimental data, all  $GW$  methods as well as the CAP-EOM-EA-CCSD approach systematically overestimate the resonance position. Furthermore,  $evGW$  and  $G_0W_0$  underestimate the resonance width by more than 0.17 eV compared to both theoretical and experimental values.

These observations strongly suggest that orbital relaxation effects, accounted for only in the qsGW method, are essential not only for reliably determining  $\eta_{opt}$  but also for accurately describing the underlying resonance state.

## 3. Spectral Function

Figure 2 compares spectral functions obtained from the qsGW method with and without the inclusion of a CAP. We focus here on the CAP-augmented qsGW (CAP-qsGW) result evaluated at the optimal CAP strength,  $\eta_{opt} = 0.0078$ , which corresponds to the lower of the two energy velocity minima discussed earlier. For comparison,

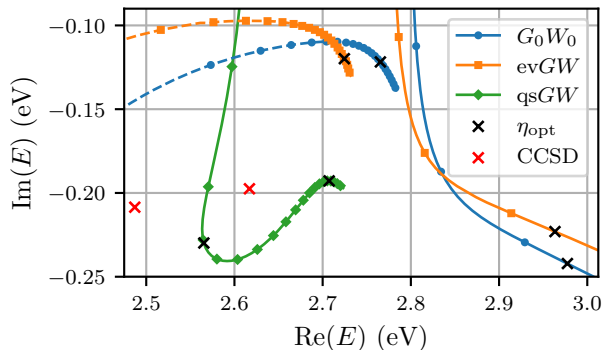


FIG. 1. Trajectories of  $N_2^-$  computed at different levels of self-consistency. For  $G_0W_0$  and  $evGW$ , the solid line denotes the trajectory associated with the first energy-velocity minimum, while the dashed line corresponds to the second minimum. Black crosses indicate the positions of the energy-velocity minima, representing the final results for the resonance state. Red crosses show the CAP-EOM-EA-CCSD reference values (see Table II). The maximum  $\eta$  value shown is 0.0155 for  $G_0W_0$  and  $evGW$ , and 0.01 for  $qsGW$ .

TABLE II. Optimal CAP strengths, resonance positions, and widths of  $N_2^-$  obtained using different methods. The  $GW$  results are from this work; other data are taken from the cited references. Optimal  $\eta$  values marked with \* are derived by another method as described in the main text.

Method	$\eta_{opt}$ (a.u.)	$E_R$ (eV)	$\Gamma$ (eV)
$G_0W_0$	0.00170*	2.977	0.484
$G_0W_0$	0.01150	2.765	0.244
$evGW$	0.00170*	2.963	0.446
$evGW$	0.01325	2.725	0.240
$qsGW$	0.00160	2.565	0.460
$qsGW$	0.00780	2.707	0.386
CAP-EOM-EA-CCSD <sup>43</sup>	0.0015	2.487	0.417
CAP-exFCI <sup>53</sup>	0.0015*	2.449	0.391
CAP-EOM-EA-CCSD <sup>179</sup>	0.0070	2.617	0.395
Experiment <sup>180</sup>		2.316	0.414

we also include spectra computed using fixed artificial broadening parameters,  $\kappa = 0.1 E_h$  and  $\kappa = 0.01 E_h$ .

While these spectral functions offer valuable qualitative insights, their physical interpretation is limited. First, the chosen Gaussian basis set is clearly too small to accurately describe the continuum, whose states are asymptotically plane-wave-like. As the basis set is enlarged by adding more diffuse functions, one would expect an increasingly dense set of discrete states approximating the continuum over a broad energy range. Second, the inclusion of the CAP discretizes the continuum by turning it into a set of complex-valued eigenvalues, with the goal of isolating resonance features. However, the CAP strength  $\eta$  was optimized only for a specific resonance state, so the resulting spectrum captures primarily this state and not

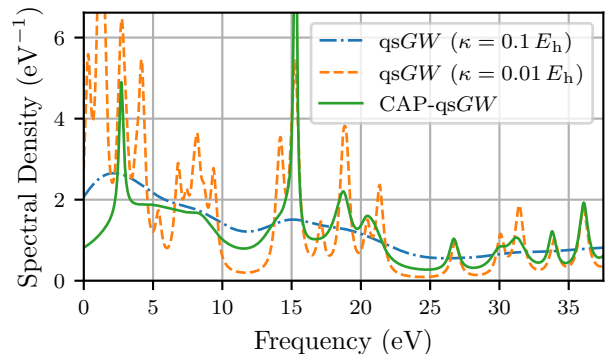


FIG. 2. Comparison of the spectral function of  $N_2$  derived by CAP-augmented  $qsGW$  (CAP- $qsGW$ ) with  $\eta_{opt} = 0.0078$  (green curve) and  $qsGW$  without CAP but with broadening parameter  $\kappa = 0.1 E_h$  (blue curve) and  $\kappa = 0.01 E_h$  (orange curve).

the entire unbound spectrum.

In the absence of a CAP, the broadening parameter  $\kappa$  uniformly widens all peaks in the spectral function, regardless of their real part  $E_R$ . As a result, increasing  $\kappa$  leads to overly broad and overlapping peaks, obscuring the identification of individual resonances. Reducing  $\kappa$  sharpens the peaks. There is no interpretation of the peak width since  $\kappa$  is an artificial parameter and not physically meaningful. All peaks are broadened with the same  $\kappa$ .

In contrast, the CAP- $qsGW$  approach yields a spectral function where each resonance is broadened according to its actual lifetime. The CAP introduces an energy-dependent, non-Hermitian perturbation that allows for a physically meaningful extraction of both the position  $E_R$  and the resonance width  $\Gamma$ . Importantly, the full width at half maximum of a given peak directly corresponds to  $\Gamma$ , the inverse lifetime of the resonance state. Hence, the inclusion of the CAP enables an identification of the metastable state and provides access to its intrinsic lifetime, a quantity inaccessible through the use of a constant broadening parameter alone.

Furthermore, it can be observed that the inclusion of the CAP leads to only a slight shift in the peak positions compared to the artificially broadened spectra. This is particularly evident for the resonance state for which the CAP strength was optimized: the first peak in the CAP- $qsGW$  spectral function. Its energy remains nearly unchanged, indicating that the CAP does not significantly alter the resonance position, but rather unveils its physical width in a controlled and interpretable manner.

## B. $CO^-$

The resonance state of  $CO^-$  is a  $^2\Pi$  shape resonance. The trajectories obtained from the different  $GW$  methods are shown in Fig. 3. In contrast to  $N_2^-$ , clear minima in

the energy velocity are identifiable at all three levels of self-consistency, as well as at the Koopmans level. However, the trajectories of  $evGW$  and  $G_0W_0$  differ markedly in shape from that of  $qsGW$ , and their minima appear at different locations along the trajectories. As a result, the optimal CAP strengths  $\eta_{opt}$  for  $evGW$  and  $G_0W_0$  are more than twice as large as that of  $qsGW$ .

The  $evGW$  and  $G_0W_0$  trajectories exhibit broad turns followed by loops in the upper right corner of the frame, corresponding to the velocity minima. In contrast, the  $qsGW$  trajectory features a much sharper turn, closely resembling the shape obtained from CAP-EOM-EA-CCSD.<sup>179</sup> This qualitative agreement suggests that orbital relaxation plays a significant role in accurately describing the resonance state of  $CO^-$ , and that  $qsGW$ , through its self-consistency in both eigenvalues and orbitals, is better suited to capture orbital relaxation. We also find another local minimum of the energy velocity at the  $qsGW$  level for  $\eta = 0.0006$ , which is less pronounced and yields a higher energy velocity than the one previously reported. Therefore, we assume it arises from the limitations of the finite basis set.

The numerical resonance parameters are summarized in Table III. As shown there,  $G_0W_0$  and  $evGW$  yield very similar results, differing by only about 0.04 eV in both the resonance position and width. Both methods, however, underestimate the width predicted by CAP-FCI and CAP-EOM-EA-CCSD by more than 0.2 eV, and deviate even more from experimental data. Additionally, they overestimate the resonance position by more than 0.25 eV compared to the theoretical references. In contrast,  $qsGW$  overestimates the theoretical reference position by less than 0.15 eV and width  $\Gamma$  by less than 0.1 eV, representing a noticeable improvement.

We compare our results to estimates of the *vertical* resonance position, that is, at the bond length of the neutral molecule, and not the adiabatic value of 1.50 eV reported in Refs. 181–183. From the parameters provided in these works, we estimated an experimental vertical resonance position of 1.93 eV, which aligns well with the cross section maximum of more recent experiments, peaking between 1.9 eV and 2.0 eV.<sup>184–186</sup> Thus, both CAP-EOM-EA-CCSD and CAP-exFCI slightly overestimate the resonance position relative to experiment. The discrepancy between  $qsGW$  and experiment is also moderate, on the order of 0.3 eV. Furthermore, for the imaginary part of the energy,  $qsGW$  provides better agreement with experimental data than the other theoretical methods.

### C. $C_2H_2^-$

The resonance state of  $C_2H_2^-$  is a  $^2\Pi_g$  shape resonance. The CAP trajectories obtained from the three  $GW$  methods are shown in Fig. 4. In contrast to the case of  $CO^-$ , all methods —  $G_0W_0$ ,  $evGW$ , and  $qsGW$  — yield qualitatively similar trajectories, characterized by smoothly curved paths with clearly defined minima in

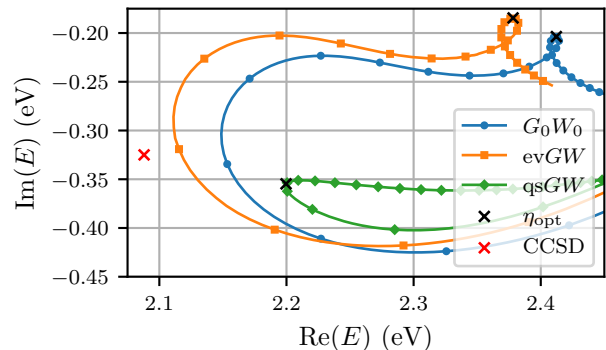


FIG. 3. Trajectories of  $CO^-$  computed at different levels of self-consistency. Black crosses indicate the positions of the energy-velocity minima, representing the final results for the resonance state. Red crosses show the CAP-EOM-EA-CCSD reference values (see Table III). The maximal  $\eta$  value shown is 0.014 for all methods.

TABLE III. Optimal CAP strengths, resonance positions, and widths of  $CO^-$  obtained using different methods. The  $GW$  results are from this work; other data are taken from the cited references. The optimal  $\eta$  value marked with \* is derived by another method as described in the main text.

Method	$\eta_{opt}$ (a.u.)	$E_R$ (eV)	$\Gamma$ (eV)
$G_0W_0$	0.00870	2.412	0.407
$evGW$	0.00875	2.378	0.369
$qsGW$	0.00295	2.200	0.709
CAP-EOM-EA-CCSD <sup>43</sup>	0.0028	2.088	0.650
CAP-exFCI <sup>53</sup>	0.0028*	2.060	0.611
Experiment <sup>181–186</sup>		1.9–2.0	–
		1.93 <sup>183</sup>	0.75 <sup>183</sup>
			0.80(3) <sup>182</sup>

the energy velocity. This similarity in shape indicates that the underlying electronic structure and its response to the CAP are treated consistently across all levels of self-consistency. Even though we find only one minimum for each method, the slope of the energy velocity decreases and then increases again around  $\eta = 0.001$ . This behavior is consistent with the pattern observed for the other molecules, where shallow local minima appear at small values of  $\eta$ .

The minor variations in the shape of the trajectories are reflected in the extracted resonance parameters (see Table IV). The optimal CAP strengths  $\eta_{opt}$  are nearly identical across methods, and the resonance positions differ by less than 0.12 eV. The computed widths  $\Gamma$  are also closely aligned, with a spread of only 0.03 eV among the methods.

All three  $GW$  variants overestimate the resonance position relative to the CAP-EOM-EA-CCSD reference (2.655 eV), with  $qsGW$  performing best among them at 2.738 eV. In terms of resonance width, all  $GW$  methods

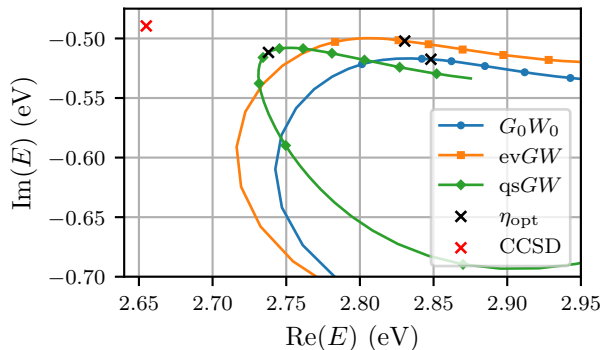


FIG. 4. Trajectories of  $\text{C}_2\text{H}_2^-$  computed at different levels of self-consistency. Black crosses indicate the positions of the energy-velocity minima, representing the final results for the resonance state. Red crosses show the CAP-EOM-EA-CCSD reference values (see Table IV). The maximal  $\eta$  value shown is 0.007 for all methods.

TABLE IV. Optimal CAP strengths, resonance positions, and widths of  $\text{C}_2\text{H}_2^-$  obtained using different methods. The  $GW$  results are from this work; other data are taken from the cited references.

Method	$\eta_{\text{opt}}$ (a.u.)	$E_{\text{R}}$ (eV)	$\Gamma$ (eV)
$G_0W_0$	0.00370	2.848	1.035
evGW	0.00365	2.830	1.004
qsGW	0.00375	2.738	1.023
CAP-EOM-EA-CCSD <sup>43</sup>	0.0036	2.655	0.979
Experiment <sup>187–191</sup>		2.5–2.6	–

predict it slightly above the CAP-EOM-EA-CCSD value of 0.979 eV, yet within deviations of 0.05 eV. Notably, the best agreement for both position and width is again achieved with qsGW, reinforcing its overall robustness.

In summary, for the  $^2\Pi_g$  resonance of  $\text{C}_2\text{H}_2^-$ , all  $GW$  methods yield consistent results, both qualitatively and quantitatively. The reduced sensitivity to the level of self-consistency indicates that this system is less impacted by orbital relaxation effects than the systems discussed before.

#### D. $\text{C}_2\text{H}_4^-$

The resonance state of  $\text{C}_2\text{H}_4^-$  corresponds to a  $^2B_{2g}$  shape resonance. The CAP trajectories obtained from the three  $GW$  variants are shown in Fig. 5. As in the case of  $\text{CO}^-$ , the  $G_0W_0$  and evGW trajectories exhibit qualitatively similar behavior, featuring broad turns with identifiable minima in the energy velocity located in the upper-right region of the portrayed frame. However, the trajectory produced by qsGW is markedly different in both shape and curvature, showing no apparent similarity to those of  $G_0W_0$  and evGW.

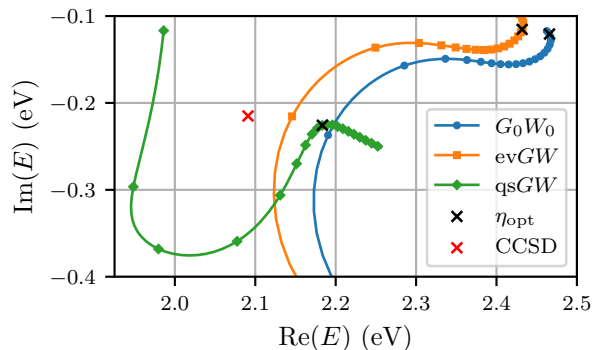


FIG. 5. Trajectories of  $\text{C}_2\text{H}_4^-$  computed at different levels of self-consistency. Black crosses indicate the positions of the energy-velocity minima, representing the final results for the resonance state. Red crosses show the CAP-EOM-EA-CCSD reference values (see Table V). The maximal  $\eta$  value shown is 0.013 for  $G_0W_0$ , 0.014 for evGW and 0.01 for qsGW.

Despite these differences in trajectory morphology, all three methods yield well-defined minima in the energy velocity. Notably, the optimal CAP strengths  $\eta_{\text{opt}}$  differ substantially:  $G_0W_0$  and evGW require relatively large values of  $\eta$  (0.01215 and 0.01055, respectively), while qsGW yields a minimum at a significantly smaller value (0.00475). This again reflects how the interaction with the CAP is handled differently at different levels of self-consistency, with qsGW requiring a weaker perturbation to stabilize the resonance state. Again, we find another local minimum on the qsGW level at lower  $\eta = 0.00095$ .

The numerical resonance parameters are summarized in Table V. The  $G_0W_0$  and evGW variants yield closely aligned results: they differ by only 0.034 eV in the resonance position and 0.01 eV in the width. However, they significantly overestimate the resonance energy and underestimate the width when compared to the high-level CAP-EOM-EA-CCSD calculation.

In contrast, qsGW produces a resonance energy of 2.183 eV and a width of 0.451 eV, in excellent agreement with the CAP-EOM-EA-CCSD reference values of 2.091 eV and 0.430 eV, respectively. All theoretical approaches overestimate the resonance position relative to experiment, likely due to limitations in the basis set and the intrinsic challenges of modeling metastable anions.

#### E. $\text{CH}_2\text{O}^-$

The resonance state of  $\text{CH}_2\text{O}^-$  corresponds to a  $^2B_1$  shape resonance. The CAP trajectories obtained from the different  $GW$  variants are shown in Fig. 6. Similar to the case of  $\text{C}_2\text{H}_4^-$ , the trajectories of  $G_0W_0$  and evGW exhibit comparable shapes, both featuring smooth curves with well-defined minima in the energy velocity. In contrast, the qsGW trajectory differs markedly in both ge-

TABLE V. Optimal CAP strengths, resonance positions, and widths of  $\text{C}_2\text{H}_4^-$  obtained using different methods. The  $GW$  results are from this work; other data are taken from the cited references.

Method	$\eta_{\text{opt}}$ (a.u.)	$E_{\text{R}}$ (eV)	$\Gamma$ (eV)
$G_0W_0$	0.01215	2.466	0.241
evGW	0.01055	2.432	0.231
qsGW	0.00475	2.183	0.451
CAP-EOM-EA-CCSD <sup>43</sup>	0.0046	2.091	0.430
Experiment <sup>192–198</sup>		1.7–1.9	$\leq 0.70$ <sup>192</sup>

ometry and curvature, reflecting the differences in orbital relaxation and self-consistency.

Despite the differences in trajectory shape, all three methods yield identifiable minima in the energy velocity, allowing for the determination of an optimal CAP strength  $\eta_{\text{opt}}$ . The values of  $\eta_{\text{opt}}$  for  $G_0W_0$  and evGW are nearly identical (0.00915 and 0.00900, respectively), while qsGW again requires a substantially smaller value (0.00450). This consistent trend across all systems studied suggests that fully self-consistent  $GW$  methods (qsGW) can stabilize resonances with weaker perturbations, owing to their more accurate treatment of orbital response in the presence of the CAP. For this molecule, we find an additional local minimum at all levels of self-consistency: at  $\eta = 0.00065$  for qsGW, and at  $\eta = 0.0013$  for the other two methods.

The corresponding resonance parameters are summarized in Table VI. As in previous systems,  $G_0W_0$  and evGW produce similar results, predicting a resonance energy of 1.597 eV and 1.554 eV, respectively, and widths of 0.213 eV and 0.179 eV. However, these methods underestimate the resonance width compared to both high-level theory and experiment.

The qsGW method yields a lower resonance position of 1.345 eV and a broader width of 0.364 eV, in excellent agreement with the CAP-EOM-EA-CCSD values of 1.352 eV and 0.376 eV, respectively. Although all  $GW$  methods overestimate the experimental resonance position, the deviation is significantly smaller for qsGW, suggesting a more realistic description of the resonance state. To the best of our knowledge, no experimental estimate for the resonance width of this system is available.

## F. $\text{CO}_2^-$

The resonance state of  $\text{CO}_2^-$  corresponds to a  $^2\Pi_u$  shape resonance. The trajectories obtained from various  $GW$  methods are shown in Fig. 7. In contrast to  $\text{CO}^-$ , the shape and behavior of the trajectories differ markedly across methods. While clear local minima in the energy velocity are observed for qsGW and  $G_0W_0$ , the evGW trajectory appears significantly less structured within the examined range. To address this, we performed additional

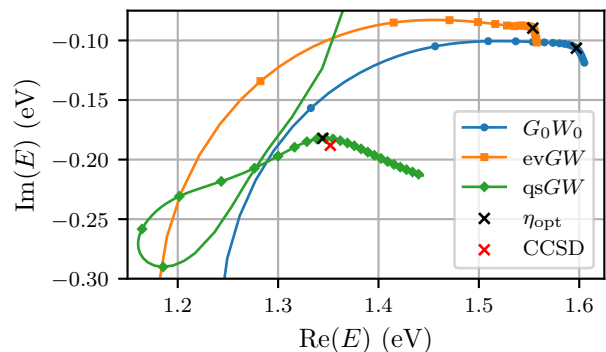


FIG. 6. Trajectories of  $\text{CH}_2\text{O}^-$  computed at different levels of self-consistency. Black crosses indicate the positions of the energy-velocity minima, representing the final results for the resonance state. Red crosses show the CAP-EOM-EA-CCSD reference values (see Table VI). The maximal  $\eta$  value shown is 0.012 for all methods.

TABLE VI. Optimal CAP strengths, resonance positions, and widths of  $\text{CH}_2\text{O}^-$  obtained using different methods. The  $GW$  results are from this work; other data are taken from the cited references.

Method	$\eta_{\text{opt}}$ (a.u.)	$E_{\text{R}}$ (eV)	$\Gamma$ (eV)
$G_0W_0$	0.00915	1.597	0.213
evGW	0.00900	1.554	0.179
qsGW	0.00450	1.345	0.364
CAP-EOM-EA-CCSD <sup>43</sup>	0.0100	1.352	0.376
Experiment <sup>199–201</sup>		0.86–0.87	–

calculations with  $s = 100$  to determine an optimal value of  $\eta$  for evGW. Subsequently, a calculation with  $s = 500$  was carried out using this optimal value.

Another related issue with evGW is that its self-consistent procedure can converge to different nearby solutions. As a result, varying  $\eta$  does not always lead to the same corresponding  $GW$  solution.<sup>176,202,203</sup> We hypothesize that this is the cause of the small bump observed in the trajectory at  $\text{Re}(E) \approx 4.0$  eV. This hypothesis is supported by the fact that no such feature appears in the  $G_0W_0$  calculation. The bump corresponds to a local minimum in the energy velocity, which we disregard due to its likely artificial origin.

In addition, as shown in the trajectory plot (see Fig. 7), the imaginary part of the evGW energy becomes positive at a certain point. This behavior is unphysical, so we restrict our search for minima to regions of the trajectory where the imaginary part remains negative.

As observed in other molecules, the qsGW trajectory features a sharp turn that leads to a well-defined minimum, located at a significantly smaller CAP strength,  $\eta_{\text{opt}} = 0.00065$ , compared to those of  $G_0W_0$  (and evGW), both of which exhibit broader trajectories and minima at  $\eta_{\text{opt}} = 0.01250$  (and 0.00960). This qualitative behavior

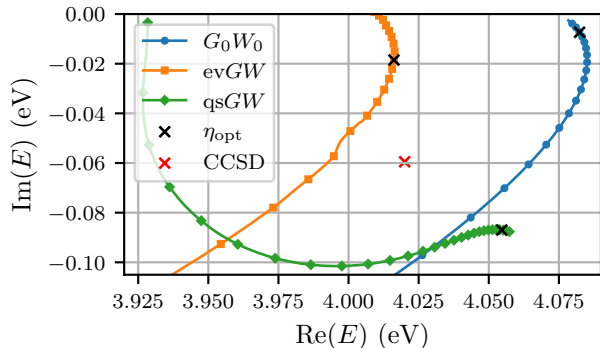


FIG. 7. Trajectories of  $\text{CO}_2^-$  computed at different levels of self-consistency. Black crosses indicate the positions of the energy-velocity minima, representing the final results for the resonance state. Red crosses show the CAP-EOM-EA-CCSD reference values (see Table VII). The maximal  $\eta$  value shown is 0.014 for  $G_0W_0$ , 0.0133 for  $evGW$  and 0.014 for  $qsGW$ .

TABLE VII. Optimal CAP strengths, resonance positions, and widths of  $\text{CO}_2^-$  obtained using different methods. The  $GW$  results are from this work; other data are taken from the cited references.

Method	$\eta_{\text{opt}}$ (a.u.)	$E_R$ (eV)	$\Gamma$ (eV)
$G_0W_0$	0.01250	4.082	0.015
$evGW$	0.00960	4.016	0.037
$qsGW$	0.01235	4.055	0.174
CAP-EOM-EA-CCSD <sup>43</sup>	0.0074	4.020	0.119
Experiment <sup>192,204–207</sup>		3.6–3.8	$0.20 \pm 0.07$ <sup>204</sup>

again highlights the stabilizing influence of quasiparticle self-consistency in  $qsGW$  and the importance of orbital relaxation for describing resonances.

The resonance parameters are collected in Table VII. At the  $qsGW$  level, the resonance position is  $E_R = 4.055$  eV with a width of  $\Gamma = 0.174$  eV, showing much closer agreement with CAP-EOM-EA-CCSD and experimental values than the other  $GW$  variants. Both the  $G_0W_0$  and  $evGW$  methods predict higher resonance positions:  $E_R = 4.082$  eV for  $G_0W_0$ , and  $E_R = 4.016$  eV for  $evGW$ . However, they significantly underestimate the resonance width:  $\Gamma = 0.037$  eV for  $evGW$ , and  $\Gamma = 0.015$  eV for  $G_0W_0$ .

$qsGW$  thus provides a much more realistic description of the metastable state in  $\text{CO}_2^-$ , both in terms of position and lifetime. While it still slightly overestimates the resonance position compared to the experimental value (between 3.6 eV and 3.8 eV), just as CAP-EOM-EA-CCSD, it reproduces the width within the experimental uncertainty ( $0.20(7)$  eV),<sup>204</sup> underlining its strength in treating resonance states where both electron correlation and orbital relaxation are essential.

## V. CONCLUSION

We have presented an implementation of the CAP formalism within the  $GW$  approximation, enabling the computation of metastable electronic resonance states in a Green’s function framework. Applied to a series of prototypical temporary anions of small systems, this approach yields both resonance positions and lifetimes through a fully complex, non-Hermitian treatment.

Among the  $GW$  variants considered, the  $qsGW$  scheme offers the most reliable performance. Across all studied molecules,  $qsGW$  reproduces CAP-EOM-EA-CCSD resonance positions within 0.11 eV and widths within 0.06 eV. The mean absolute differences are only 0.07 eV for the position and 0.03 eV for the width.  $qsGW$  systematically overestimates the resonance position relative to CAP-EOM-EA-CCSD, except for  $\text{CH}_2\text{O}$ , where it slightly underestimates it by only 0.007 eV. No clear trend emerges for the widths.

In contrast,  $G_0W_0$  and  $evGW$  consistently underestimate resonance widths and predict larger optimal CAP strengths, indicating stronger perturbative effects. These methods also struggle to resolve shallow or less pronounced minima in the CAP energy trajectories, limiting their robustness. Notably,  $evGW$ , which includes eigenvalue self-consistency, offers a modest improvement in resonance positions compared to  $G_0W_0$ , but this trend does not extend to the lifetimes.

These findings highlight the importance of orbital relaxation, which is fully accounted for only in  $qsGW$ . The close agreement of  $qsGW$  with wavefunction benchmarks suggests that a self-consistent treatment of both eigenvalues and orbitals is critical for a robust description of metastable states. Although all theoretical methods, including CAP-EOM-EA-CCSD, tend to overestimate experimental resonance positions,  $qsGW$  provides accuracy on par with high-level wavefunction theory, delivering reliable estimates for both positions and lifetimes. Thus,  $qsGW$  offers a promising and comparatively cheap alternative for describing resonances in larger molecules, where wavefunction-based methods would be too expensive.

This work opens several avenues for further development. Incorporating first-order perturbative corrections to the CAP energy may enhance reliability, as demonstrated in wavefunction-based approaches.<sup>43</sup> For  $G_0W_0$  and  $evGW$ , exploring alternative starting points, such as Kohn-Sham orbitals,<sup>208</sup> could help mitigate current shortcomings. Furthermore, it would be worthwhile to investigate various flavors of the closely related GF2 (or second Born) methods,<sup>173,209–226</sup> which circumvent solving the RPA eigenvalue problem by employing an excitation energy and amplitude ansatz based on quasiparticle energies and orbitals. Given their structural similarity to the CAP- $GW$  approach introduced in this work, extending these methods with a CAP should be straightforward and potentially more computationally efficient. This would also be closely related to the CAP-ADC methods discussed in the introduction.<sup>63–65,81</sup>

Finally, the methodology presented here could be extended to other metastable phenomena, such as core-ionization and Auger-Meitner decay, where accurate lifetimes are particularly important. However, the *GW* formalism is likely not suited for describing Feshbach resonances, which involve two-particle processes, as it is well known that *GW* struggles to accurately capture satellite transitions.<sup>82,227</sup>

## SUPPORTING INFORMATION

The [Supporting Information](#) contains, for each system considered here, the molecular coordinates, the exponents of the additional diffuse basis functions, the representation of the Dyson orbital associated with the resonance state, the behavior of the energy-velocity as a function of  $\eta$ , and the spectral functions.

## ACKNOWLEDGEMENTS

The authors would like to thank Josep Alberola, Antoine Marie, Ivan Duchemin, and Xavier Blase for insightful discussions. This project has received funding from the European Research Council (ERC) under the European Union’s Horizon 2020 research and innovation programme (Grant agreement No. 863481). This work used the HPC resources from CALMIP (Toulouse) under allocations 2025-18005.

## Appendix A: SRG renormalization for complex $qsGW$

We extended the SRG renormalization method<sup>153</sup> for complex-valued energies, which yields the following matrix elements of the self-energy

$$\begin{aligned} [\tilde{\Sigma}_c]_{pq} = & \sum_{iv} \frac{(\tilde{\epsilon}_{piv} + \tilde{\epsilon}_{qiv})N_{pqiv}}{\tilde{\epsilon}_{piv}^2 + \tilde{\epsilon}_{qiv}^2 + \tilde{\kappa}_{piv}^2 + \tilde{\kappa}_{qiv}^2} \\ & + \sum_{av} \frac{(\tilde{\epsilon}_{pav} + \tilde{\epsilon}_{qav})N_{pqav}}{\tilde{\epsilon}_{pav}^2 + \tilde{\epsilon}_{qav}^2 + \tilde{\kappa}_{pav}^2 + \tilde{\kappa}_{qav}^2} \\ & + i \sum_{iv} \frac{(\tilde{\kappa}_{piv} + \tilde{\kappa}_{qiv})N_{pqiv}}{\tilde{\epsilon}_{piv}^2 + \tilde{\epsilon}_{qiv}^2 + \tilde{\kappa}_{piv}^2 + \tilde{\kappa}_{qiv}^2} \\ & - i \sum_{av} \frac{(\tilde{\kappa}_{pav} + \tilde{\kappa}_{qav})N_{pqav}}{\tilde{\epsilon}_{pav}^2 + \tilde{\epsilon}_{qav}^2 + \tilde{\kappa}_{pav}^2 + \tilde{\kappa}_{qav}^2} \end{aligned} \quad (\text{A1})$$

with the real and imaginary parts of the denominator in Eq. (17)

$$\tilde{\epsilon}_{pqv} = \text{Re}\{\epsilon_p - \epsilon_q - \text{sgn}[\text{Re}(\epsilon_q - \mu)]\Omega_\nu\} \quad (\text{A2a})$$

$$\tilde{\kappa}_{pqv} = \kappa + \text{Im}\{\text{sgn}[\text{Re}(\epsilon_q - \mu)](\epsilon_p - \epsilon_q) - \Omega_\nu\} \quad (\text{A2b})$$

(where  $\mu$  is the chemical potential) and the renormalized elements

$$N_{pqr\nu} = M_{pr,\nu}M_{qr,\nu} \left[ 1 - e^{-s(\tilde{\epsilon}_{pr\nu}^2 + \tilde{\epsilon}_{qr\nu}^2 + \tilde{\kappa}_{pr\nu}^2 + \tilde{\kappa}_{qr\nu}^2)} \right] \quad (\text{A3})$$

The exponential term in the renormalized density ensures that the numerator tends faster to zero when both the real and imaginary parts of the denominator tend to zero.

## REFERENCES

- <sup>1</sup>K. D. Jordan and P. D. Burrow, “Temporary Anion States of Polyatomic Hydrocarbons,” *Chem. Rev.* **87**, 557–588 (1987).
- <sup>2</sup>K. D. Jordan and F. Wang, “Theory of Dipole-Bound Anions,” *Annu. Rev. Phys. Chem.* **54**, 367–396 (2003).
- <sup>3</sup>J. Simons, “Molecular Anions,” *J. Phys. Chem. A* **112**, 6401–6511 (2008).
- <sup>4</sup>J. Simons, “Theoretical Study of Negative Molecular Ions,” *Annu. Rev. Phys. Chem.* **62**, 107–128 (2011).
- <sup>5</sup>K. D. Jordan, V. K. Voora, and J. Simons, “Negative Electron Affinities From Conventional Electronic Structure Methods,” *Theor. Chem. Acc.* **133**, 1445 (2014).
- <sup>6</sup>J. Simons, “Detachment Processes For Molecular Anions,” in *Advanced Series in Physical Chemistry: Photoionization and Photodetachment* (World Scientific Publishing Co.: Singapore, 2000) pp. 958–1010.
- <sup>7</sup>J. Simons, “Molecular anions perspective,” *J. Phys. Chem. A* **127**, 3940–3957 (2023).
- <sup>8</sup>B. Boudaiffa, P. Cloutier, D. Hunting, M. A. Huels, and L. Sanche, “Resonant Formation of DNA Strand Breaks by Low-Energy (3 to 20 eV) Electrons,” *Science* **287**, 1658–1660 (2000).
- <sup>9</sup>F. Martin, P. D. Burrow, Z. Cai, P. Cloutier, D. Hunting, and L. Sanche, “DNA Strand Breaks Induced by 0–4 eV Electrons: The Role of Shape Resonances,” *Phys. Rev. Lett.* **93**, 068101 (2004).
- <sup>10</sup>J. Simons, “How Do Low-Energy (0.1–2 eV) Electrons Cause DNA-Strand Breaks?” *Acc. Chem. Res.* **39**, 772–779 (2006).
- <sup>11</sup>E. Alizadeh, T. M. Orlando, and L. Sanche, “Biomolecular Damage Induced by Ionizing Radiation: The Direct and Indirect Effects of Low-Energy Electrons on DNA,” *Annu. Rev. Phys. Chem.* **66**, 379–398 (2015).
- <sup>12</sup>N. I. Hammer, J.-W. Shin, J. M. Headrick, E. G. Diken, J. R. Roscioli, G. H. Weddle, and M. A. Johnson, “How Do Small Water Clusters Bind an Excess Electron?” *Science* **306**, 675–679 (2004).
- <sup>13</sup>C. J. Clarke and J. R. Verlet, “Dynamics of anions: From bound to unbound states and everything in between,” *Annu. Rev. Phys. Chem.* **75**, 89–110 (2024).
- <sup>14</sup>G. Gamow, “Zur Quantentheorie des Atomkernes,” *Z. Phys.* **51**, 204–212 (1928).
- <sup>15</sup>A. J. F. Siegert, “On the Derivation of the Dispersion Formula for Nuclear Reactions,” *Phys. Rev.* **56**, 750–752 (1939).
- <sup>16</sup>S. Klaiman and I. Gilary, “On Resonance: A First Glimpse into the Behavior of Unstable States,” *Adv. Quantum Chem.* **63**, 1–31 (2012).
- <sup>17</sup>D. Zuev, K. B. Bravaya, T. D. Crawford, R. Lindh, and A. I. Krylov, “Electronic structure of the two isomers of the anionic form of p-coumaric acid chromophore,” *J. Chem. Phys.* **134**, 034310 (2011).
- <sup>18</sup>K. B. Bravaya, D. Zuev, E. Epifanovsky, and A. I. Krylov, “Complex-Scaled Equation-Of-Motion Coupled-Cluster Method with Single and Double Substitutions for Autoionizing Excited States: Theory, Implementation, and Examples,” *J. Chem. Phys.* **138**, 124106 (2013).
- <sup>19</sup>A. A. Kunitsa and K. B. Bravaya, “First-Principles Calculations of the Energy and Width of the  $^2A_u$  Shape Resonance in p-Benzoquinone: A Gateway State for Electron Transfer,” *J. Phys. Chem. Lett.* **6**, 1053–1058 (2015).
- <sup>20</sup>H. Feshbach, “Unified Theory of Nuclear Reactions,” *Ann. Phys.* **5**, 357–390 (1958).
- <sup>21</sup>H. Feshbach, “A Unified Theory of Nuclear Reactions. II,” *Ann. Phys.* **19**, 287–313 (1962).

- <sup>22</sup>W. Domcke, "Theory of resonance and threshold effects in electron-molecule collisions: The projection-operator approach," *Phys. Rep.* **208**, 97–188 (1991).
- <sup>23</sup>V. Averbukh and L. S. Cederbaum, "Ab initio calculation of interatomic decay rates by a combination of the fano ansatz, green's-function methods, and the stieltjes imaging technique," *J. Chem. Phys.* **123**, 204107 (2005).
- <sup>24</sup>P. Kolorenč, V. Averbukh, K. Gokhberg, and L. S. Cederbaum, "Ab initio calculation of interatomic decay rates of excited doubly ionized states in clusters," *J. Chem. Phys.* **129**, 244102 (2008).
- <sup>25</sup>J. Kolorenc and L. Mitas, "Applications of quantum Monte Carlo methods in condensed systems," *Rep. Prog. Phys.* **74**, 026502 (2011).
- <sup>26</sup>S. Yabushita and C. W. McCurdy, "Feshbach resonances in electron-molecule scattering by the complex multiconfiguration scf and configuration interaction procedures: The  $1\sigma_g^+$  autoionizing states of  $\text{H}_2$ ," *J. Chem. Phys.* **83**, 3547–3559 (1985).
- <sup>27</sup>Y. Sajeev, V. Vysotskiy, L. S. Cederbaum, and N. Moiseyev, "Continuum remover-complex absorbing potential: Efficient removal of the nonphysical stabilization points," *J. Chem. Phys.* **131**, 211102 (2009).
- <sup>28</sup>J. Schiedt and R. Weinkauff, "Resonant photodetachment via shape and feshbach resonances: p-benzoquinone anions as a model system," *J. Chem. Phys.* **110**, 304–314 (1999).
- <sup>29</sup>A. A. Kunitsa and K. B. Bravaya, "Electronic structure of the para-benzoquinone radical anion revisited," *Phys. Chem. Chem. Phys.* **18**, 3454–3462 (2016).
- <sup>30</sup>A. A. Kunitsa, A. A. Granovsky, and K. B. Bravaya, "CAP-XMCQDPT2 Method for Molecular Electronic Resonances," *J. Chem. Phys.* **146**, 184107 (2017).
- <sup>31</sup>A. Loupas and J. D. Gorfinkiel, "Resonances in low-energy electron scattering from para-benzoquinone," *Phys. Chem. Chem. Phys.* **19**, 18252–18261 (2017).
- <sup>32</sup>R. F. da Costa, J. C. Ruivo, F. Kossoski, M. T. d. N. Varella, M. H. F. Bettega, D. B. Jones, M. J. Brunger, and M. A. P. Lima, "An ab initio investigation for elastic and electronically inelastic electron scattering from para-benzoquinone," *J. Chem. Phys.* **149**, 174308 (2018).
- <sup>33</sup>B. Sedmidubská and J. Kočíšek, "Interaction of low-energy electrons with radiosensitizers," *Phys. Chem. Chem. Phys.* **26**, 9112–9136 (2024).
- <sup>34</sup>Q. T. Wu, H. Anderson, A. K. Watkins, D. Arora, K. Barnes, M. Padovani, C. N. Shingledecker, C. R. Arumainayagam, and J. B. R. Battat, "Role of Low-Energy (<20 eV) Secondary Electrons in the Extraterrestrial Synthesis of Prebiotic Molecules," *ACS Earth Space Chem.* **8**, 79–88 (2024).
- <sup>35</sup>C. R. Arumainayagam, H.-L. Lee, R. B. Nelson, D. R. Haines, and R. P. Gunawardane, "Low-energy electron-induced reactions in condensed matter," *Surf. Sci. Rep.* **65**, 1–44 (2010).
- <sup>36</sup>R. M. Thorman, R. K. T. P., D. H. Fairbrother, and O. Ingólfsson, "The role of low-energy electrons in focused electron beam induced deposition: four case studies of representative precursors," *Beilstein J. Nanotechnol.* **6**, 1904–1926 (2015).
- <sup>37</sup>T.-C. Jagau, K. B. Bravaya, and A. I. Krylov, "Extending Quantum Chemistry of Bound States to Electronic Resonances," *Annu. Rev. Phys. Chem.* , 525–553 (2017).
- <sup>38</sup>T.-C. Jagau, "Theory of electronic resonances: fundamental aspects and recent advances," *Chem. Commun.* **58**, 5205–5224 (2022).
- <sup>39</sup>G. Jolicard and E. J. Austin, "Optical potential stabilisation method for predicting resonance levels," *Chem. Phys. Lett.* **121**, 106–110 (1985).
- <sup>40</sup>U. V. Riss and H.-D. Meyer, "Calculation of resonance energies and widths using the complex absorbing potential method," *J. Phys. B: At. Mol. Opt. Phys.* **26**, 4503 (1993).
- <sup>41</sup>T. Sommerfeld, U. V. Riss, H.-D. Meyer, L. S. Cederbaum, B. Engels, and H. U. Suter, "Temporary anions - calculation of energy and lifetime by absorbing potentials: the resonance," *J. Phys. B: At. Mol. Opt. Phys.* **31**, 4107 (1998).
- <sup>42</sup>A. Ghosh, N. Vaval, and S. Pal, "Equation-of-motion coupled-cluster method for the study of shape resonance," *J. Chem. Phys.* **136**, 234110 (2012).
- <sup>43</sup>D. Zuev, T.-C. Jagau, K. B. Bravaya, E. Epifanovsky, Y. Shao, E. Sundstrom, M. Head-Gordon, and A. I. Krylov, "Complex Absorbing Potentials Within EOM-CC Family of Methods: Theory, Implementation, and Benchmarks," *J. Chem. Phys.* **141**, 024102 (2014).
- <sup>44</sup>T.-C. Jagau, D. Zuev, K. B. Bravaya, E. Epifanovsky, and A. I. Krylov, "A Fresh Look at Resonances and Complex Absorbing Potentials: Density Matrix-Based Approach," *J. Phys. Chem. Lett.* **5**, 310–315 (2014).
- <sup>45</sup>T.-C. Jagau and A. I. Krylov, "Complex Absorbing Potential Equation-of-Motion Coupled-Cluster Method Yields Smooth and Internally Consistent Potential Energy Surfaces and Lifetimes for Molecular Resonances," *J. Phys. Chem. Lett.* **5**, 3078–3085 (2014).
- <sup>46</sup>T. Sommerfeld and M. Ehara, "Complex absorbing potentials with voronoi isosurfaces wrapping perfectly around molecules," *J. Chem. Theory Comput.* **11**, 4627–4633 (2015).
- <sup>47</sup>J. A. Gyamfi and T.-C. Jagau, "A New Strategy to Optimize Complex Absorbing Potentials for the Computation of Resonance Energies and Widths," *J. Chem. Theory Comput.* **20**, 1096–1107 (2024).
- <sup>48</sup>E. Balslev and J. M. Combes, "Spectral properties of many-body Schrödinger operators with dilatation-analytic interactions," *Commun. Math. Phys.* **22**, 280–294 (1971).
- <sup>49</sup>N. Moiseyev, "Quantum theory of resonances: calculating energies, widths and cross-sections by complex scaling," *Phys. Rep.* **302**, 212–293 (1998).
- <sup>50</sup>C. W. McCurdy and T. N. Rescigno, "Extension of the method of complex basis functions to molecular resonances," *Phys. Rev. Lett.* **41**, 1364–1368 (1978).
- <sup>51</sup>A. F. White, M. Head-Gordon, and C. W. McCurdy, "Complex basis functions revisited: Implementation with applications to carbon tetrafluoride and aromatic N-containing heterocycles within the static-exchange approximation," *J. Chem. Phys.* **142**, 054103 (2015).
- <sup>52</sup>N. Moiseyev, *Non-Hermitian Quantum Mechanics* (Cambridge University Press, Cambridge, England, UK, 2011).
- <sup>53</sup>Y. Damour, A. Scemama, F. Kossoski, and P.-F. Loos, "Selected Configuration Interaction for Resonances," *J. Phys. Chem. Lett.* **15**, 8296–8305 (2024).
- <sup>54</sup>A. Ghosh, A. Karne, S. Pal, and N. Vaval, "CAP/EOM-CCSD method for the study of potential curves of resonant states," *Phys. Chem. Chem. Phys.* **15**, 17915–17921 (2013).
- <sup>55</sup>Y. Sajeev, R. Santra, and S. Pal, "Analytically continued Fock space multireference coupled-cluster theory: Application to the  $\text{Ilg}_2$  shape resonance in e-N2 scattering," *J. Chem. Phys.* **122**, 234320 (2005).
- <sup>56</sup>Y. Sajeev and S. Pal, "A general formalism of the Fock space multireference coupled cluster method for investigating molecular electronic resonances," *Mol. Phys.* **103**, 2267–2275 (2005).
- <sup>57</sup>T.-C. Jagau, "Non-iterative triple excitations in equation-of-motion coupled-cluster theory for electron attachment with applications to bound and temporary anions," *J. Chem. Phys.* **148**, 024104 (2018).
- <sup>58</sup>I. Jana, S. Basumallick, S. Pal, and N. Vaval, "Resonance study: Effect of partial triples excitation using complex absorbing potential-based Fock-space multi-reference coupled cluster," *Int. J. Quantum Chem.* **121**, e26738 (2021).
- <sup>59</sup>M. Ehara and T. Sommerfeld, "CAP/SAC-CI method for calculating resonance states of metastable anions," *Chem. Phys. Lett.* **537**, 107–112 (2012).
- <sup>60</sup>Q. M. Phung, Y. Komori, T. Yanai, T. Sommerfeld, and M. Ehara, "Combination of a Voronoi-Type Complex Absorbing Potential with the XMS-CASPT2 Method and Pilot Applications," *J. Chem. Theory Comput.* **16**, 2606–2616 (2020).
- <sup>61</sup>T. Sommerfeld and R. Santra, "Efficient method to perform CAP/CI calculations for temporary anions," *Int. J. Quantum*

- Chem.* **82**, 218–226 (2001).
- <sup>62</sup>Y. Zhou and M. Ernzerhof, “Calculating the lifetimes of metastable states with complex density functional theory,” *J. Phys. Chem. Lett.* **3**, 1916–1920 (2012).
- <sup>63</sup>R. Santra and L. S. Cederbaum, “Complex absorbing potentials in the framework of electron propagator theory. I. General formalism,” *J. Chem. Phys.* **117**, 5511–5521 (2002).
- <sup>64</sup>S. Feuerbacher, T. Sommerfeld, R. Santra, and L. S. Cederbaum, “Complex absorbing potentials in the framework of electron propagator theory. II. Application to temporary anions,” *J. Chem. Phys.* **118**, 6188–6199 (2003).
- <sup>65</sup>S. Feuerbacher and R. Santra, “Calculating molecular Rydberg states using the one-particle Green’s function: Application to HCO and C(NH<sub>2</sub>)<sub>3</sub>,” *J. Chem. Phys.* **123**, 194310 (2005).
- <sup>66</sup>A. M. Belogolova, A. L. Dempwolff, A. Dreuw, and A. B. Trofimov, “A complex absorbing potential electron propagator approach to resonance states of metastable anions,” *J. Phys. Conf. Ser.* **1847**, 012050 (2021).
- <sup>67</sup>J. Schirmer, A. B. Trofimov, and G. Stelter, “A non-Dyson third-order approximation scheme for the electron propagator,” *J. Chem. Phys.* **109**, 4734–4744 (1998).
- <sup>68</sup>J. Schirmer, *Many-Body Methods for Atoms, Molecules and Clusters* (Springer, 2018).
- <sup>69</sup>R. M. Martin, L. Reining, and D. M. Ceperley, *Interacting Electrons: Theory and Computational Approaches* (Cambridge University Press, 2016).
- <sup>70</sup>G. Csanak, H. Taylor, and R. Yaris, “Green’s function technique in atomic and molecular physics,” in *Advances in atomic and molecular physics*, Vol. 7 (Elsevier, 1971) pp. 287–361.
- <sup>71</sup>A. L. Fetter and J. D. Waleck, *Quantum Theory of Many Particle Systems* (McGraw Hill, San Francisco, 1971).
- <sup>72</sup>L. Hedin, “New method for calculating the one-particle Green’s function with application to the electron-gas problem,” *Phys. Rev.* **139**, A796 (1965).
- <sup>73</sup>D. Golze, M. Dvorak, and P. Rinke, “The GW Compendium: A Practical Guide to Theoretical Photoemission Spectroscopy,” *Front. Chem.* **7**, 377 (2019).
- <sup>74</sup>A. Marie, A. Ammar, and P.-F. Loos, “The GW approximation: A quantum chemistry perspective,” in *Advances in Quantum Chemistry*, Novel Treatments of Strong Correlations, Vol. 90 (2024) pp. 157–184.
- <sup>75</sup>M. F. Falchetta, L. A. DiFalco, D. S. Ackerman, J. C. Barlow, and K. D. Jordan, “Assessment of various electronic structure methods for characterizing temporary anion states: Application to the ground state anions of n<sub>2</sub>, c<sub>2</sub>h<sub>2</sub>, c<sub>2</sub>h<sub>4</sub>, and c<sub>6</sub>h<sub>6</sub>,” *J. Phys. Chem. A* **118**, 7489–7497 (2014).
- <sup>76</sup>M. J. van Setten, F. Caruso, S. Sharifzadeh, X. Ren, M. Scheffler, F. Liu, J. Lischner, L. Lin, J. R. Deslippe, S. G. Louie, C. Yang, F. Weigend, J. B. Neaton, F. Evers, and P. Rinke, “GW 100: Benchmarking  $G_0W_0$  for Molecular Systems,” *J. Chem. Theory Comput.* **11**, 5665–5687 (2015).
- <sup>77</sup>F. Caruso, M. Dauth, M. J. van Setten, and P. Rinke, “Benchmark of GW Approaches for the GW100 Test Set,” *J. Chem. Theory Comput.* **12**, 5076 (2016).
- <sup>78</sup>K. Krause and W. Klopper, “Implementation of the bethe-salpeter equation in the turbomole program,” *J. Comput. Chem.* **38**, 383–388 (2017).
- <sup>79</sup>A. M. Lewis and T. C. Berkelbach, “Vertex corrections to the polarizability do not improve the gw approximation for the ionization potential of molecules,” *J. Chem. Theory Comput.* **15**, 2925 (2019).
- <sup>80</sup>F. Bruneval, N. Dattani, and M. J. van Setten, “The GW Miracle in Many-Body Perturbation Theory for the Ionization Potential of Molecules,” *Front. Chem.* **9**, 749779 (2021).
- <sup>81</sup>E. Monino and P.-F. Loos, “Connections and performances of green’s function methods for charged and neutral excitations,” *J. Chem. Phys.* **159**, 034105 (2023).
- <sup>82</sup>A. Marie and P.-F. Loos, “Reference Energies for Valence Ionizations and Satellite Transitions,” *J. Chem. Theory Comput.* **20**, 4751–4777 (2024).
- <sup>83</sup>M. J. van Setten, R. Costa, F. Viñes, and F. Illas, “Assessing GW Approaches for Predicting Core Level Binding Energies,” *J. Chem. Theory Comput.* **14**, 877–883 (2018).
- <sup>84</sup>D. Golze, J. Wilhelm, M. J. van Setten, and P. Rinke, “Core-Level Binding Energies from GW: An Efficient Full-Frequency Approach within a Localized Basis,” *J. Chem. Theory Comput.* **14**, 4856–4869 (2018).
- <sup>85</sup>D. Golze, L. Keller, and P. Rinke, “Accurate Absolute and Relative Core-Level Binding Energies from GW,” *J. Phys. Chem. Lett.* **11**, 1840–1847 (2020).
- <sup>86</sup>D. Mejia-Rodriguez, A. Kunitsa, E. Aprà, and N. Govind, “Scalable Molecular GW Calculations: Valence and Core Spectra,” *J. Chem. Theory Comput.* **17**, 7504–7517 (2021).
- <sup>87</sup>J. Li, Y. Jin, P. Rinke, W. Yang, and D. Golze, “Benchmark of gw methods for core-level binding energies,” *J. Chem. Theory Comput.* **18**, 7570–7585 (2022).
- <sup>88</sup>I. Mukatayev, F. Moevus, B. Sklénard, V. Olevano, and J. Li, “XPS Core-Level Chemical Shift by Ab Initio Many-Body Theory,” *J. Phys. Chem. A* **127**, 1642–1648 (2023).
- <sup>89</sup>R. L. Panadés-Barrueta and D. Golze, “Accelerating Core-Level GW Calculations by Combining the Contour Deformation Approach with the Analytic Continuation of W,” *J. Chem. Theory Comput.* **19**, 5450–5464 (2023).
- <sup>90</sup>G. Baym and L. P. Kadanoff, “Conservation laws and correlation functions,” *Phys. Rev.* **124**, 287–299 (1961).
- <sup>91</sup>G. Baym, “Self-consistent approximations in many-body systems,” *Phys. Rev.* **127**, 1391–1401 (1962).
- <sup>92</sup>C. De Dominicis and P. C. Martin, “Stationary entropy principle and renormalization in normal and superfluid systems. i. algebraic formulation,” *J. Math. Phys.* **5**, 14–30 (1964).
- <sup>93</sup>C. De Dominicis and P. C. Martin, “Stationary entropy principle and renormalization in normal and superfluid systems. ii. diagrammatic formulation,” *J. Math. Phys.* **5**, 31–59 (1964).
- <sup>94</sup>N. E. Bickers, D. J. Scalapino, and S. R. White, “Conserving Approximations for Strongly Correlated Electron Systems: Bethe-Salpeter Equation and Dynamics for the Two-Dimensional Hubbard Model,” *Phys. Rev. Lett.* **62**, 961–964 (1989).
- <sup>95</sup>N. Bickers and D. Scalapino, “Conserving approximations for strongly fluctuating electron systems. I. Formalism and calculational approach,” *Ann. Phys.* **193**, 206–251 (1989).
- <sup>96</sup>N. E. Bickers and S. R. White, “Conserving approximations for strongly fluctuating electron systems. II. Numerical results and parquet extension,” *Phys. Rev. B* **43**, 8044–8064 (1991).
- <sup>97</sup>L. Hedin, “On correlation effects in electron spectroscopies and the GW approximation,” *J. Phys. Condens. Matter* **11**, R489–R528 (1999).
- <sup>98</sup>N. E. Bickers, “Self-Consistent Many-Body Theory for Condensed Matter Systems,” in *Theoretical Methods for Strongly Correlated Electrons*, edited by D. Sénéchal, A.-M. Tremblay, and C. Bourbonnais (Springer New York, New York, NY, 2004) pp. 237–296.
- <sup>99</sup>E. L. Shirley, “Self-consistent gw and higher-order calculations of electron states in metals,” *Phys. Rev. B* **54**, 7758–7764 (1996).
- <sup>100</sup>R. Del Sole, L. Reining, and R. W. Godby, “GWT Approximation for Electron Self-Energies in Semiconductors and Insulators,” *Phys. Rev. B* **49**, 8024–8028 (1994).
- <sup>101</sup>A. Schindlmayr and R. W. Godby, “Systematic Vertex Corrections through Iterative Solution of Hedin’s Equations Beyond the  $\{\text{GW}\}$  Approximation,” *Phys. Rev. Lett.* **80**, 1702–1705 (1998).
- <sup>102</sup>A. J. Morris, M. Stankovski, K. T. Delaney, P. Rinke, P. García-González, and R. W. Godby, “Vertex corrections in localized and extended systems,” *Phys. Rev. B* **76**, 155106 (2007).
- <sup>103</sup>M. Shishkin, M. Marsman, and G. Kresse, “Accurate Quasiparticle Spectra from Self-Consistent GW Calculations with Vertex Corrections,” *Phys. Rev. Lett.* **99**, 246403 (2007).
- <sup>104</sup>P. Romaniello, S. Guyot, and L. Reining, “The self-energy beyond GW: Local and nonlocal vertex corrections,” *J. Chem. Phys.* **131**, 154111 (2009).

- <sup>105</sup>P. Romaniello, F. Bechstedt, and L. Reining, "Beyond the *GW* Approximation: Combining Correlation Channels," *Phys. Rev. B* **85**, 155131 (2012).
- <sup>106</sup>A. Grüneis, G. Kresse, Y. Hinuma, and F. Oba, "Ionization potentials of solids: The importance of vertex corrections," *Phys. Rev. Lett.* **112**, 096401 (2014).
- <sup>107</sup>L. Hung, F. Bruneval, K. Baishya, and S. Ögüt, "Benchmarking the *GW* Approximation and Bethe–Salpeter Equation for Groups IB and IIB Atoms and Monoxides," *J. Chem. Theory Comput.* **13**, 2135–2146 (2017).
- <sup>108</sup>E. Maggio and G. Kresse, "*GW* Vertex Corrected Calculations for Molecular Systems," *J. Chem. Theory Comput.* **13**, 4765–4778 (2017).
- <sup>109</sup>C. Mejuto-Zaera and V. c. v. Vlcek, "Self-consistency in *GWT* formalism leading to quasiparticle-quasiparticle couplings," *Phys. Rev. B* **106**, 165129 (2022).
- <sup>110</sup>M. Wen, V. Abraham, G. Harsha, A. Shee, B. Whaley, and D. Zgid, "Comparing Self-Consistent *GW* and Vertex Corrected  $G_0W_0$  Accuracy for Molecular Ionization Potentials," *J. Chem. Theory Comput.*, in press (2024).
- <sup>111</sup>F. Bruneval and A. Förster, "Fully Dynamic  $G_3W_2$  Self-Energy for Finite Systems: Formulas and Benchmark," *J. Chem. Theory Comput.* **20**, 3218–3230 (2024).
- <sup>112</sup>A. Förster and F. Bruneval, "Why Does the *GW* Approximation Give Accurate Quasiparticle Energies? The Cancellation of Vertex Corrections Quantified," *J. Phys. Chem. Lett.* **15**, 12526–12534 (2024).
- <sup>113</sup>A. Förster, "Beyond Quasi-Particle Self-Consistent *GW* for Molecules with Vertex Corrections," *J. Chem. Theory Comput.* **21**, 1709–1721 (2025).
- <sup>114</sup>D. Neuhauser, E. Rabani, and R. Baer, "Expeditious stochastic calculation of random-phase approximation energies for thousands of electrons in three dimensions," *J. Phys. Chem. Lett.* **4**, 1172–1176 (2013).
- <sup>115</sup>D. Neuhauser, Y. Gao, C. Arntsen, C. Karshenas, E. Rabani, and R. Baer, "Breaking the Theoretical Scaling Limit for Predicting Quasiparticle Energies: The Stochastic *GW* Approach," *Phys. Rev. Lett.* **113**, 076402 (2014).
- <sup>116</sup>M. Kaltak, J. Klimeš, and G. Kresse, "Low scaling algorithms for the random phase approximation: Imaginary time and laplace transformations," *J. Chem. Theory Comput.* **10**, 2498–2507 (2014).
- <sup>117</sup>M. Govoni and G. Galli, "Large Scale *GW* Calculations," *J. Chem. Theory Comput.* **11**, 2680–2696 (2015).
- <sup>118</sup>V. Vlček, E. Rabani, D. Neuhauser, and R. Baer, "Stochastic *GW* Calculations for Molecules," *J. Chem. Theory Comput.* **13**, 4997–5003 (2017).
- <sup>119</sup>J. Wilhelm, D. Golze, L. Talirz, J. Hutter, and C. A. Pignedoli, "Toward *GW* Calculations on Thousands of Atoms," *J. Phys. Chem. Lett.* **9**, 306–312 (2018).
- <sup>120</sup>I. Duchemin and X. Blase, "Separable resolution-of-the-identity with all-electron gaussian bases: Application to cubic-scaling rpa," *J. Chem. Phys.* **150**, 174120 (2019).
- <sup>121</sup>M. D. Ben, F. H. da Jornada, A. Canning, N. Wichmann, K. Raman, R. Sasanka, C. Yang, S. G. Louie, and J. Deslippe, "Large-scale *GW* calculations on pre-exascale HPC systems," *Comp. Phys. Comm.* **235**, 187–195 (2019).
- <sup>122</sup>A. Förster and L. Visscher, "Low-Order Scaling  $G_0W_0$  by Pair Atomic Density Fitting," *J. Chem. Theory Comput.* **16**, 7381–7399 (2020).
- <sup>123</sup>I. Duchemin and X. Blase, "Robust analytic-continuation approach to many-body *GW* calculations," *J. Chem. Theory Comput.* **16**, 1742–1756 (2020).
- <sup>124</sup>M. Kaltak and G. Kresse, "Minimax isometry method: A compressive sensing approach for matsubara summation in many-body perturbation theory," *Phys. Rev. B* **101**, 205145 (2020).
- <sup>125</sup>A. Förster and L. Visscher, "Low-Order Scaling Quasiparticle Self-Consistent *GW* for Molecules," *Front. Chem.* **9**, 736591 (2021).
- <sup>126</sup>I. Duchemin and X. Blase, "Cubic-scaling all-electron gw calculations with a separable density-fitting space–time approach," *J. Chem. Theory Comput.* **17**, 2383–2393 (2021).
- <sup>127</sup>J. Wilhelm, P. Seewald, and D. Golze, "Low-Scaling *GW* with Benchmark Accuracy and Application to Phosphorene Nanosheets," *J. Chem. Theory Comput.* **17**, 1662–1677 (2021).
- <sup>128</sup>A. Förster and L. Visscher, "Quasiparticle Self-Consistent  $GW$ -Bethe–Salpeter Equation Calculations for Large Chromophoric Systems," *J. Chem. Theory Comput.* **18**, 6779–6793 (2022).
- <sup>129</sup>V. W.-z. Yu and M. Govoni, "GPU Acceleration of Large-Scale Full-Frequency *GW* Calculations," *J. Chem. Theory Comput.* **18**, 4690–4707 (2022).
- <sup>130</sup>J. Tölle, N. Niemeier, and J. Neugebauer, "Accelerating analytic-continuation gw calculations with a laplace transform and natural auxiliary functions," *J. Chem. Theory Comput.* **20**, 2022–2032 (2024).
- <sup>131</sup>L. Gallandi, N. Marom, P. Rinke, and T. Körzdörfer, "Accurate Ionization Potentials and Electron Affinities of Acceptor Molecules II: Non-Empirically Tuned Long-Range Corrected Hybrid Functionals," *J. Chem. Theory Comput.* **12**, 605–614 (2016).
- <sup>132</sup>R. M. Richard, M. S. Marshall, O. Dolgounitcheva, J. V. Ortiz, J.-L. Brédas, N. Marom, and C. D. Sherrill, "Accurate Ionization Potentials and Electron Affinities of Acceptor Molecules I. Reference Data at the CCSD(T) Complete Basis Set Limit," *J. Chem. Theory Comput.* **12**, 595–604 (2016).
- <sup>133</sup>J. W. Knight, X. Wang, L. Gallandi, O. Dolgounitcheva, X. Ren, J. V. Ortiz, P. Rinke, T. Körzdörfer, and N. Marom, "Accurate Ionization Potentials and Electron Affinities of Acceptor Molecules III: A Benchmark of *GW* Methods," *J. Chem. Theory Comput.* **12**, 615–626 (2016).
- <sup>134</sup>O. Dolgounitcheva, M. Díaz-Tinoco, V. G. Zakrzewski, R. M. Richard, N. Marom, C. D. Sherrill, and J. V. Ortiz, "Accurate Ionization Potentials and Electron Affinities of Acceptor Molecules IV: Electron-Propagator Methods," *J. Chem. Theory Comput.* **12**, 627–637 (2016).
- <sup>135</sup>G. Strinati, H. J. Mattausch, and W. Hanke, "Dynamical correlation effects on the quasiparticle bloch states of a covalent crystal," *Phys. Rev. Lett.* **45**, 290–294 (1980).
- <sup>136</sup>M. S. Hybertsen and S. G. Louie, "First-Principles Theory of Quasiparticles: Calculation of Band Gaps in Semiconductors and Insulators," *Phys. Rev. Lett.* **55**, 1418–1421 (1985).
- <sup>137</sup>R. W. Godby, M. Schlüter, and L. J. Sham, "Self-energy operators and exchange-correlation potentials in semiconductors," *Phys. Rev. B* **37**, 10159–10175 (1988).
- <sup>138</sup>W. von der Linden and P. Horsch, "Precise quasiparticle energies and hartree-fock bands of semiconductors and insulators," *Phys. Rev. B* **37**, 8351–8362 (1988).
- <sup>139</sup>J. E. Northrup, M. S. Hybertsen, and S. G. Louie, "Many-body Calculation of the Surface-State Energies for Si(111)2×1," *Phys. Rev. Lett.* **66**, 500–503 (1991).
- <sup>140</sup>X. Blase, X. Zhu, and S. G. Louie, "Self-energy effects on the surface-state energies of h-si(111)1×1," *Phys. Rev. B* **49**, 4973–4980 (1994).
- <sup>141</sup>M. Rohlfing, P. Krüger, and J. Pollmann, "Efficient Scheme for *GW* Quasiparticle Band-Structure Calculations with Applications to Bulk Si and to the Si(001)-(2×1) Surface," *Phys. Rev. B* **52**, 1905–1917 (1995).
- <sup>142</sup>M. S. Hybertsen and S. G. Louie, "Electron correlation in semiconductors and insulators: Band gaps and quasiparticle energies," *Phys. Rev. B* **34**, 5390–5413 (1986).
- <sup>143</sup>M. Shishkin and G. Kresse, "Self-Consistent *GW* Calculations for Semiconductors and Insulators," *Phys. Rev. B* **75**, 235102 (2007).
- <sup>144</sup>X. Blase and C. Attaccalite, "Charge-transfer excitations in molecular donor-acceptor complexes within the many-body bethe-salpeter approach," *Appl. Phys. Lett.* **99**, 171909 (2011).
- <sup>145</sup>C. Faber, C. Attaccalite, V. Olevano, E. Runge, and X. Blase, "First-principles *GW* calculations for DNA and RNA nucleobases," *Phys. Rev. B* **83**, 115123 (2011).

- <sup>146</sup>T. Rangel, S. M. Hamed, F. Bruneval, and J. B. Neaton, “Evaluating the *GW* Approximation with CCSD(T) for Charged Excitations Across the Oligoacenes,” *J. Chem. Theory Comput.* **12**, 2834–2842 (2016).
- <sup>147</sup>X. Gui, C. Holzer, and W. Klopper, “Accuracy assessment of gw starting points for calculating molecular excitation energies using the bethe–salpeter formalism,” *J. Chem. Theory Comput.* **14**, 2127–2136 (2018).
- <sup>148</sup>S. V. Faleev, M. van Schilfgaarde, and T. Kotani, “All-Electron Self-Consistent *G W* Approximation: Application to Si, MnO, and NiO,” *Phys. Rev. Lett.* **93**, 126406 (2004).
- <sup>149</sup>M. van Schilfgaarde, T. Kotani, and S. Faleev, “Quasiparticle Self-Consistent *G W* Theory,” *Phys. Rev. Lett.* **96**, 226402 (2006).
- <sup>150</sup>T. Kotani, M. van Schilfgaarde, and S. V. Faleev, “Quasiparticle self-consistent *G W* method: A basis for the independent-particle approximation,” *Phys. Rev. B* **76**, 165106 (2007).
- <sup>151</sup>S.-H. Ke, “All-electron *G W* methods implemented in molecular orbital space: Ionization energy and electron affinity of conjugated molecules,” *Phys. Rev. B* **84**, 205415 (2011).
- <sup>152</sup>F. Kaplan, M. E. Harding, C. Seiler, F. Weigend, F. Evers, and M. J. van Setten, “Quasi-Particle Self-Consistent *GW* for Molecules,” *J. Chem. Theory Comput.* **12**, 2528–2541 (2016).
- <sup>153</sup>A. Marie and P.-F. Loos, “A Similarity Renormalization Group Approach to Green’s Function Methods,” *J. Chem. Theory Comput.* **19**, 3943–3957 (2023).
- <sup>154</sup>N. Moiseyev, P. R. Certain, and F. Weinhold, “Resonance properties of complex-rotated hamiltonians,” *Mol. Phys.* **36**, 1613–1630 (1978).
- <sup>155</sup>Let  $\tilde{C}(\eta)$  be the matrix of non-orthonormal eigenvectors, i.e., the results of a diagonalisation method for non-Hermitian complex matrices. Then, to ensure the normalization condition, we perform an adapted Cholesky decomposition to get a lower triangular matrix  $L$  fulfilling  $\tilde{C}(\eta)^T \cdot S \cdot \tilde{C}(\eta) = L \cdot L^T$ . Then, to obtain the orthonormalized eigenvectors, we transform the original coefficients matrix using the inverse transpose of the Cholesky factor  $L$ , as follows:  $C(\eta) = \tilde{C}(\eta)L^{-T}$ .
- <sup>156</sup>P. Pulay, “Convergence Acceleration of Iterative Sequences. The Case of SCF Iteration,” *Chem. Phys. Lett.* **73**, 393–398 (1980).
- <sup>157</sup>P. Pulay, “Improved SCF convergence acceleration,” *J. Comput. Chem.* **3**, 556–560 (1982).
- <sup>158</sup>R. Santra, L. Cederbaum, and H.-D. Meyer, “Electronic decay of molecular clusters: non-stationary states computed by standard quantum chemistry methods,” *Chem. Phys. Lett.* **303**, 413–419 (1999).
- <sup>159</sup>F. Aryasetiawan and O. Gunnarsson, “The *GW* Method,” *Rep. Prog. Phys.* **61**, 237–312 (1998).
- <sup>160</sup>G. Onida, L. Reining, and A. Rubio, “Electronic excitations: Density-functional versus many-body green’s function approaches,” *Rev. Mod. Phys.* **74**, 601–659 (2002).
- <sup>161</sup>L. Reining, “The *GW* Approximation: Content, Successes and Limitations,” *WIREs Comput. Mol. Sci.* **8**, e1344 (2017).
- <sup>162</sup>W. H. Dickhoff and D. V. Neck, *Many-Body Theory Exposed!* (World Scientific, 2008).
- <sup>163</sup>R. Starke and G. Kresse, “Self-consistent Green function equations and the hierarchy of approximations for the four-point propagator,” *Phys. Rev. B* **85**, 075119 (2012).
- <sup>164</sup>R. Orlando, P. Romaniello, and P.-F. Loos, “The three channels of many-body perturbation theory: *GW*, particle–particle, and electron–hole *T*-matrix self-energies,” *J. Chem. Phys.* **159**, 184113 (2023).
- <sup>165</sup>A. Marie, P. Romaniello, and P.-F. Loos, “Anomalous propagators and the particle–particle channel: Hedin’s equations,” *Phys. Rev. B* **110**, 115155 (2024).
- <sup>166</sup>A. Marie, P. Romaniello, X. Blase, and P.-F. Loos, “Anomalous propagators and the particle–particle channel: Bethe–Salpeter equation,” *J. Chem. Phys.* **162**, 134105 (2025).
- <sup>167</sup>D. Bohm and D. Pines, “A Collective Description of Electron Interactions. I. Magnetic Interactions,” *Phys. Rev.* **82**, 625–634 (1951).
- <sup>168</sup>D. Pines and D. Bohm, “A Collective Description of Electron Interactions: II. Collective vs Individual Particle Aspects of the Interactions,” *Phys. Rev.* **85**, 338–353 (1952).
- <sup>169</sup>D. Bohm and D. Pines, “A Collective Description of Electron Interactions: III. Coulomb Interactions in a Degenerate Electron Gas,” *Phys. Rev.* **92**, 609–625 (1953).
- <sup>170</sup>P. Nozières and D. Pines, “Correlation Energy of a Free Electron Gas,” *Phys. Rev.* **111**, 442–454 (1958).
- <sup>171</sup>C. Holzer, A. M. Teale, F. Hampe, S. Stopkowicz, T. Helgaker, and W. Klopper, “*GW* Quasiparticle Energies of Atoms in Strong Magnetic Fields,” *J. Chem. Phys.* **150**, 214112 (2019).
- <sup>172</sup>Practically, we ensure the normalization of the RPA eigenvectors with the same method as introduced in the HF section, i.e., by a Cholesky decomposition of
- $$\begin{pmatrix} X & Y \\ Y & X \end{pmatrix}^T \cdot \begin{pmatrix} 1 & 0 \\ 0 & -1 \end{pmatrix} \cdot \begin{pmatrix} X & Y \\ Y & X \end{pmatrix}$$
- <sup>173</sup>A. Szabo and N. S. Ostlund, *Modern quantum chemistry* (McGraw-Hill, New York, 1989).
- <sup>174</sup>P. F. Loos, “QuAck: a software for emerging quantum electronic structure methods,” (2019), <https://github.com/pfloos/QuAck>.
- <sup>175</sup>J. Gayvert, “Opencap: An open-source program for studying resonances in molecules,” (2024), commit: 1562fce. Accessed: 2025-04-28.
- <sup>176</sup>M. Vèril, P. Romaniello, J. A. Berger, and P. F. Loos, “Unphysical discontinuities in gw methods,” *J. Chem. Theory Comput.* **14**, 5220 (2018).
- <sup>177</sup>B. M. Nestmann and S. D. Peyerimhoff, “CI method for determining the location and width of resonances in electron-molecule collision processes,” *J. Phys. B: At. Mol. Phys.* **18**, 4309 (1985).
- <sup>178</sup>M. Vèril, A. Scemama, M. Caffarel, F. Lipparini, M. Boggio-Pasqua, D. Jacquemin, and P.-F. Loos, “QUESTDB: A database of highly accurate excitation energies for the electronic structure community,” *WIREs Comput. Mol. Sci.* **11**, e1517.
- <sup>179</sup>J. R. Gayvert and K. B. Bravaya, “Projected CAP-EOM-CCSD method for electronic resonances,” *J. Chem. Phys.* **156**, 094108 (2022).
- <sup>180</sup>M. Berman, H. Estrada, L. S. Cederbaum, and W. Domcke, “Nuclear dynamics in resonant electron-molecule scattering beyond the local approximation: The 2.3-eV shape resonance in N<sub>2</sub>,” *Phys. Rev. A* **28**, 1363–1381 (1983).
- <sup>181</sup>H. Ehrhardt, L. Langhans, F. Linder, and H. S. Taylor, “Resonance Scattering of Slow Electrons from H<sub>2</sub> and CO Angular Distributions,” *Phys. Rev.* **173**, 222–230 (1968).
- <sup>182</sup>M. Zubek and C. Szmytkowski, “Calculation of resonant vibrational excitation of CO by scattering of electrons,” *J. Phys. B: At. Mol. Phys.* **10**, L27 (1977).
- <sup>183</sup>M. Zubek and C. Szmytkowski, “Electron impact vibrational excitation of CO in the range 1–4 eV,” *Phys. Lett. A* **74**, 60–62 (1979).
- <sup>184</sup>S. J. Buckman and B. Lohmann, “Electron scattering from co in the <sup>2</sup>I resonance region,” *Phys. Rev. A* **34**, 1561–1563 (1986).
- <sup>185</sup>C. Szmytkowski, K. Maciag, and G. Karwasz, “Absolute electron-scattering total cross section measurements for noble gas atoms and diatomic molecules,” *Phys. Scr.* **54**, 271 (1996).
- <sup>186</sup>M. Allan, “Electron collisions with co: Elastic and vibrational excitation cross sections,” *Phys. Rev. A* **81**, 042706 (2010).
- <sup>187</sup>K. H. Kochem, W. Sohn, K. Jung, H. Ehrhardt, and E. S. Chang, “Direct and resonant vibrational excitation of C<sub>2</sub>H<sub>2</sub> by electron impact from 0 to 3.6 eV,” *J. Phys. B At. Mol. Opt. Phys.* **18**, 1253 (1985).
- <sup>188</sup>K. D. Jordan and P. D. Burrow, “Studies of the Temporary Anion States of Unsaturated Hydrocarbons by Electron Transmission Spectroscopy,” *Acc. Chem. Res.* **11**, 341–348 (1978).
- <sup>189</sup>R. Dressler and M. Allan, “A dissociative electron attachment, electron transmission, and electron energy-loss study of the temporary negative ion of acetylene,” *J. Chem. Phys.* **87**, 4510–4518 (1987).

- <sup>190</sup>L. Andric and R. I. Hall, "Resonance phenomena observed in electron scattering from acetylene," *J. Phys. B At. Mol. Opt. Phys.* **21**, 355 (1988).
- <sup>191</sup>C. Szmytkowski, P. Mozejko, M. Zawadzki, K. Maciag, and E. d. z. Ptasińska Denga, "Electron-scattering cross sections for selected alkyne molecules: Measurements and calculations," *Phys. Rev. A* **89**, 052702 (2014).
- <sup>192</sup>L. Sanche and G. J. Schulz, "Electron transmission spectroscopy: Resonances in triatomic molecules and hydrocarbons," *J. Chem. Phys.* **58**, 479–493 (1973).
- <sup>193</sup>I. C. Walker, A. Stamatovic, and S. F. Wong, "Vibrational excitation of ethylene by electron impact: 1–11 eV," *J. Chem. Phys.* **69**, 5532–5537 (1978).
- <sup>194</sup>S. L. Lunt, J. Randell, J. P. Ziesel, G. Mrotzek, and D. Field, "Low-energy electron scattering from  $\text{CH}_4$ ,  $\text{C}_2\text{H}_4$  and  $\text{C}_2\text{H}_6$ ," *J. Phys. B At. Mol. Opt. Phys.* **27**, 1407 (1994).
- <sup>195</sup>R. Panajotovic, M. Kitajima, H. Tanaka, M. Jelisavcic, J. Lower, L. Campbell, M. J. Brunger, and S. J. Buckman, "Electron collisions with ethylene," *J. Phys. B At. Mol. Opt. Phys.* **36**, 1615 (2003).
- <sup>196</sup>C. Szmytkowski, S. Kwitniewski, and E. d. z. Ptasińska Denga, "Electron collisions with tetrafluoroethylene ( $\text{C}_2\text{F}_4$ ) and ethylene ( $\text{C}_2\text{H}_4$ ) molecules," *Phys. Rev. A* **68**, 032715 (2003).
- <sup>197</sup>M. Allan, C. Winstead, and V. McKoy, "Electron scattering in ethene: Excitation of the  $a^3B_{1u}$  state, elastic scattering, and vibrational excitation," *Phys. Rev. A* **77**, 042715 (2008).
- <sup>198</sup>M. A. Khakoo, S. M. Khakoo, A. Sakaamini, B. A. Hlousek, L. R. Hargreaves, J. Lee, and R. Murase, "Low-energy elastic electron scattering from ethylene: Elastic scattering and vibrational excitation," *Phys. Rev. A* **93**, 012710 (2016).
- <sup>199</sup>P. Burrow and J. Micejda, "Electron transmission study of the formaldehyde electron affinity," *Chem. Phys. Lett.* **42**, 223–226 (1976).
- <sup>200</sup>E. Van Veen, W. Van Dijk, and H. Brongersma, "Low-energy electron-impact excitation spectra of formaldehyde, acetaldehyde and acetone," *Chem. Phys.* **16**, 337–345 (1976).
- <sup>201</sup>C. Benoit and R. Abouaf, "Low-energy electron collisions with formaldehyde: interference phenomena in the differential vibrational excitation cross section," *Chem. Phys. Lett.* **123**, 134–138 (1986).
- <sup>202</sup>P.-F. Loos, A. Scemama, I. Duchemin, D. Jacquemin, and X. Blase, "Pros and Cons of the Bethe–Salpeter Formalism for Ground-State Energies," *J. Phys. Chem. Lett.* **11**, 3536–3545 (2020).
- <sup>203</sup>E. Monino and P.-F. Loos, "Unphysical discontinuities, intruder states and regularization in *GW* methods," *J. Chem. Phys.* **156**, 231101 (2022).
- <sup>204</sup>P. D. Burrow and L. Sanche, "Elastic Scattering of Low-Energy Electrons at  $180^\circ$  in  $\text{CO}_2$ ," *Phys. Rev. Lett.* **28**, 333–336 (1972).
- <sup>205</sup>M. J. W. Boness and G. J. Schulz, "Vibrational excitation in  $\text{CO}_2$  via the 3.8-eV resonance," *Phys. Rev. A* **9**, 1969–1979 (1974).
- <sup>206</sup>M. Allan, "Selectivity in the excitation of fermi-coupled vibrations in  $\text{CO}_2$  by impact of slow electrons," *Phys. Rev. Lett.* **87**, 033201 (2001).
- <sup>207</sup>A. I. Lozano, A. García-Abenza, F. Blanco Ramos, M. Hasan, D. S. Slaughter, T. Weber, R. P. McEachran, R. D. White, M. J. Brunger, P. Limão-Vieira, and G. García Gómez-Tejedor, "Electron and Positron Scattering Cross Sections from  $\text{CO}_2$ : A Comparative Study over a Broad Energy Range (0.1–5000 eV)," *J. Phys. Chem. A* **126**, 6032–6046 (2022).
- <sup>208</sup>F. Bruneval and M. A. L. Marques, "Benchmarking the Starting Points of the *GW* Approximation for Molecules," *J. Chem. Theory Comput.* **9**, 324–329 (2013).
- <sup>209</sup>S. Suhai, "Quasiparticle energy-band structures in semiconducting polymers: Correlation effects on the band gap in polyacetylene," *Phys. Rev. B* **27**, 3506–3518 (1983).
- <sup>210</sup>L. J. Holleboom and J. G. Snijders, "A Comparison between the Moller-Plesset and Green's Function Perturbative Approaches to the Calculation of the Correlation Energy in the Many-electron Problem," *J. Chem. Phys.* **93**, 5826–5837 (1990).
- <sup>211</sup>M. E. Casida and D. P. Chong, "Physical interpretation and assessment of the Coulomb-hole and screened-exchange approximation for molecules," *Phys. Rev. A* **40**, 4837–4848 (1989).
- <sup>212</sup>M. E. Casida and D. P. Chong, "Simplified Green-function approximations: Further assessment of a polarization model for second-order calculation of outer-valence ionization potentials in molecules," *Phys. Rev. A* **44**, 5773–5783 (1991).
- <sup>213</sup>G. Stefanucci and R. van Leeuwen, *Nonequilibrium Many-Body Theory of Quantum Systems: A Modern Introduction* (Cambridge University Press, Cambridge, 2013).
- <sup>214</sup>J. V. Ortiz, "Electron propagator theory: An approach to prediction and interpretation in quantum chemistry: Electron propagator theory," *WIREs Comput. Mol. Sci.* **3**, 123–142 (2013).
- <sup>215</sup>J. J. Phillips and D. Zgid, "Communication: The Description of Strong Correlation within Self-Consistent Green's Function Second-Order Perturbation Theory," *J. Chem. Phys.* **140**, 241101 (2014).
- <sup>216</sup>J. J. Phillips, A. A. Kananenka, and D. Zgid, "Fractional Charge and Spin Errors in Self-Consistent Green's Function Theory," *J. Chem. Phys.* **142**, 194108 (2015).
- <sup>217</sup>A. A. Rusakov, J. J. Phillips, and D. Zgid, "Local Hamiltonians for Quantitative Green's Function Embedding Methods," *J. Chem. Phys.* **141**, 194105 (2014).
- <sup>218</sup>A. A. Rusakov and D. Zgid, "Self-Consistent Second-Order Green's Function Perturbation Theory for Periodic Systems," *J. Chem. Phys.* **144**, 054106 (2016).
- <sup>219</sup>S. Hirata, M. R. Hermes, J. Simons, and J. V. Ortiz, "General-Order Many-Body Green's Function Method," *J. Chem. Theory Comput.* **11**, 1595–1606 (2015).
- <sup>220</sup>S. Hirata, A. E. Doran, P. J. Knowles, and J. V. Ortiz, "One-particle many-body Green's function theory: Algebraic recursive definitions, linked-diagram theorem, irreducible-diagram theorem, and general-order algorithms," *J. Chem. Phys.* **147**, 044108 (2017).
- <sup>221</sup>O. J. Backhouse, A. Santana-Bonilla, and G. H. Booth, "Scalable and predictive spectra of correlated molecules with moment truncated iterated perturbation theory," *J. Phys. Chem. Lett.* **12**, 7650–7658 (2021).
- <sup>222</sup>O. J. Backhouse and G. H. Booth, "Efficient excitations and spectra within a perturbative renormalization approach," *J. Chem. Theory Comput.* **16**, 6294–6304 (2020).
- <sup>223</sup>O. J. Backhouse, M. Nusspickel, and G. H. Booth, "Wave function perspective and efficient truncation of renormalized second-order perturbation theory," *J. Chem. Theory Comput.* **16**, 1090–1104 (2020).
- <sup>224</sup>P. Pokhilko and D. Zgid, "Interpretation of multiple solutions in fully iterative GF2 and GW schemes using local analysis of two-particle density matrices," *J. Chem. Phys.* **155**, 024101 (2021).
- <sup>225</sup>P. Pokhilko, S. Isakov, C.-N. Yeh, and D. Zgid, "Evaluation of two-particle properties within finite-temperature self-consistent one-particle Green's function methods: Theory and application to *GW* and *GF2*," *J. Chem. Phys.* **155**, 024119 (2021).
- <sup>226</sup>P. Pokhilko, C.-N. Yeh, and D. Zgid, "Iterative subspace algorithms for finite-temperature solution of Dyson equation," *J. Chem. Phys.* **156**, 094101 (2022).
- <sup>227</sup>P.-F. Loos, A. Marie, and A. Ammar, "Cumulant Green's function methods for molecules," *Faraday Discuss.* **254**, 240–260 (2024).